Atypical phosphatases drive dissolved organic phosphorus utilization by phosphorus-stressed phytoplankton in the California Current Ecosystem

Viktoria Steck[1,2]*, Robert H. Lampe[3,4], Simran Bhakta[1], Kimberly Camarena Marrufo[1], Jamee C. Adams[1], Eesha Sachdev[1], Andrew E. Allen[3,4], Julia M. Diaz[1]*

[1] Geosciences Research Division, Scripps Institution of Oceanography, University of California San Diego, La Jolla, CA 92093, United States
[2] Department of Marine Chemistry and Biogeochemistry, Woods Hole Oceanographic Institution, Woods Hole, MA 02543, United States
[3] Integrative Oceanography Division, Scripps Institution of Oceanography, University of California San Diego, La Jolla, CA 92093, United States
[4] Microbial and Environmental Genomics, J. Craig Venter Institute, La Jolla, CA 92037, United States

*Corresponding authors:
Viktoria Steck, Department of Marine Chemistry and Geochemistry, Woods Hole Oceanographic Institution, 266 Woods Hole Road, Woods Hole, MA 02543, USA. Email: viktoria.steck@whoi.edu
Julia M. Diaz, Geosciences Research Division, Scripps Institution of Oceanography, University of California San Diego, 9500 Gilman Drive, La Jolla, CA 92093, United States. Email: j2diaz@scripps.edu

Abstract

In the ocean, dissolved organic phosphorus (DOP) supports the health and productivity of marine phytoplankton, a phenomenon most often investigated under inorganic phosphate (Pi) scarcity. However, microbial DOP acquisition in Pi replete environments remains poorly understood. Here, we conducted a combination of nutrient addition experiments, alkaline phosphatase (AP) rate measurements, and metatranscriptomics along an onshore-to-offshore gradient in the California Current Ecosystem (CCE), an upwelling region relatively replete in Pi. We found that AP activity (APA) and eukaryotic gene transcripts for DOP utilization were present throughout the CCE. In bottle incubations, APA was upregulated in response to iron (Fe) and nitrogen (N) additions. Major contributors to these trends included atypical alkaline phosphatases (AP_{aty}) of diatoms in upwelling areas, and unclassified phosphodiesterases (other PDE) of multiple eukaryotic taxa in offshore regimes. APA and gene expression dynamics were not coupled to phytoplankton growth, suggesting that phytoplankton experience underlying P stress, or a state of cellular metabolism caused by Pi scarcity, even in regions primarily growth-limited by other elements. AP_{aty} and PDE (other) genes were highly abundant among the microbial community phosphatase pool, highlighting the importance of detecting these atypical and unclassified proteins via manual curation of metatranscriptomics data. Altogether, these results emphasize the functional diversity of phosphatases sustaining microbial community health in diverse and productive marine habitats.

Introduction

Phosphorus (P) is a nutrient essential for marine phytoplankton, which contribute up to ~50% of the global net primary production (*1*). The form of dissolved organic phosphorus (DOP) constitutes the majority of available P in the world's large oligotrophic ocean gyres (*2*). Previously thought to be utilized only in times of inorganic phosphate (Pi or PO_4^{3-}) scarcity, it is now recognized that DOP supports marine microbial nutrition and primary productivity across various ocean environments (*2*), including nutrient-rich coastal areas (*3-5*). However, the mechanisms governing microbial DOP utilization across different trophic regimes are poorly understood.

Marine microbes produce hydrolytic enzymes to access DOP, which often require metal cofactors to function and thus link the P cycle with environmental trace metals (*2*). One widespread enzyme family are alkaline phosphatases (APs), containing zinc (Zn) in the isoform PhoA (*6*) and iron (Fe) in PhoX and PhoD (*7, 8*), plus unusual metal requirements such as Co (*9*). Indeed, microbial AP activity (APA) was found to be limited by Fe or Zn availability in North Atlantic communities (*10, 11*). DOP also supports a substantial fraction of microbial productivity in Pacific subtropical gyres (*12, 13*), albeit with overall lower hydrolysis rates than in the Atlantic (*10*), potentially due to less trace metal inputs through dust fluxes (*14*). While one study in the North Pacific detected elevated expression of Zn-dependent *phoA* in Fe-limited colonies of the diazotroph *Trichodesmium* sp. (*15*), the relationship between P nutrition and trace metals in the Pacific remains unclear.

Ambient DOP consists of P-esters (P-O-C bonds, 80-85% of bulk DOP; ex. P-sugars, P-lipids, nucleotides), P-anhydrides (P-O-P, 8-13%; ex. nucleoside di- and triphosphates, pyro-P, poly-P), and phosphonates (C-P, 5-10%; ex. phosphonolipids, small molecule metabolites) (*16*). In order to access this chemically diverse nutrient reservoir, phytoplankton need to produce a large functional variety of different enzymes (*2*). Besides APs, which hydrolyze P-monoesters (*10*), several classes of P-diesterases (PDE) and -triesterases (PTER), many of which are responsive to Pi availability (*17, 18*), are expressed by marine microbes. More recently, proteins degrading P-anhydrides and phosphonates have gained attention as these compounds were found widely bioavailable to marine plankton (*19-24*). The P-anhydrases nucleoside triphosphatases (5'-NT) and inorganic pyrophosphatases (*ppa*) are implicated in the growth of diatoms under low Pi (*20*), and some nucleoside diphosphate (NUDIX) hydrolases upregulated under Pi scarcity (*18*). Together with polyphosphatases (*ppk*, *ppx*), 5'-NTs are also used by heterotrophs to acquire P and/or carbon-containing byproducts (*25, 26*).

Here, we provide novel physiological and transcriptional insights into DOP utilization within natural mixed microbial communities experiencing several interwoven nutrient stressors between the North Pacific Subtropical Gyre and the California Current Ecosystem (CCE). The CCE is an eastern boundary current upwelling system with a high variability of ecological zones, fluctuating nutrient availabilities, and characteristically high and diatom-driven productivity (*27*). Large parts of the central CCE are perpetually nitrogen (N)-limited, but experience seasonal and intermittent Fe-limitation especially during coastal upwelling episodes and in transition zones (*28-30*). Pi can reach low surface concentrations (<0.1 μM) in transition domains (*31*) and become biologically limiting in the stratified oligotrophic North Pacific subtropical gyre (*32*). The ability to metabolize DOP buffers phytoplankton against nutrient stress (*33*), and further deciphering how DOP supports marine microorganism communities in the face of environmental changes is vital for improving primary production and climate predictions. This is especially important in light of these Pacific ecosystem's increasing stressors of altered nutrient stoichiometry (*34*), marine heatwaves (*27*), water column hypoxia, and ocean acidification (*28*).

Methods

Field sampling

Sampling was conducted on two expeditions in the California Current in June 2020 aboard the R/V Sally Ride (SR2003) and in July-August 2021 aboard the R/V Roger Revelle (P2107). The P2107 expedition was part of the California Current Ecosystem (CCE) Long-Term Ecological Research (LTER) program and used drifters for quasi-Lagrangian tracking of discrete water parcels as described previously for LTER cruises in the CCE (*35*). Each series of measurements during continuous tracking of one water mass was denoted a Lagrangian cycle. For comparison to other studies from P2107, station 1 corresponds to the cycle 1, station 2 to cycle 2, station 3 to the California Current Transect, and station 4 to cycle 3 (**Fig. 1**). The SR2003 expedition served one station at 32.51304 N and 118.21386 W. On P2107, seawater for dissolved inorganic nutrients was collected using a SBE911+ CTD system mounted in a 24-place 10 L Niskin rosette with an SBE32 carousel (Sea-Bird Electronics). On both expeditions, trace metal clean seawater was collected using single acid-cleaned, Teflon-coated 12 L GO-Flo bottles (General Oceanics) mounted directly on non-metallic hydroline (Amsteel) triggered with acid-cleaned Teflon messengers designed by Ken Bruland (SR2003), or 5 L X-Niskin bottles (Ocean Test Equipment) mounted on a powder-coated rosette deployed on kevlar-coated hydrowire (SpaceLay) (P2107). Sampling at subsurface chlorophyll layers was conducted at the depth below the top of the nitracline, determined by the nitrate-sensors ISUS (SR2003) or SUNA (P2107) mounted on the CTD rosette, which did not always correspond to the depth of maximum Chl *a* concentration (see **Fig. S1**). This region was previously identified to have higher Fe stress due to mismatched stoichiometric supply of N and Fe from diapycnal mixing (*29*).

Field incubations

Shipboard bottle incubations at stations 1-4 (**Fig. 1**) were set up under positive pressure with HEPA-filtered air in a trace metal clean plastic bubble (SR2003) or UNOLS trace metal clean van (P2107). Metal stock solutions were prepared as 1.5 µM ($CoCl_2 \cdot 6H_2O$) or 15 µM ($FeCl_3 \cdot 6H_2O$, $ZnSO_4 \cdot 7H_2O$, $MnSO_4 \cdot 6H_2O$) in 2% HCl. Nutrient stock solutions ($NaNO_3$, NH_4Cl) were prepared as 15 mM in H_2O, treated with Chelex for 24 hours, and 0.2 µm-filtered prior to use. Polycarbonate bottles, previously cleaned with 1% Citranox followed by 10% HCl (optima grade, Fischer Scientific) for at least two weeks each, were rinsed three times, filled with seawater, and spiked with combinations of the trace metals (final concentrations): Fe (5 nM), Zn (5 nM), Co (0.5 nM), and nitrogen (+N) as both NO_3^{2-} (5 mM) and NH_4^+ (5 mM). At P2107 stations 1-4, 1 L polycarbonate bottles (n = 12) were treated in triplicate with +Fe, +N, +Fe+N, including an unamended control. At SR2003, 60 mL polycarbonate flasks (n = 24) were treated in triplicate with +Fe, +Zn, +Co, +N, +Fe+N, +Zn+N, +Co+N, plus an unamended control. The bottles were incubated on-deck in circulating seawater from the ship's underway intake and covered with neutral density screening to mimic in situ temperature and light conditions at the sample collection depth, as confirmed with a PAR sensor. At the end of each incubation experiment (48h), the incubation bottles were sampled for chlorophyll *a*, dissolved P pools, cell counts, APA, and transcriptomics.

Chlorophyll

Seawater (100 mL) was filtered onto 25 mm GF/F glass fiber filters (Whatman), and filters were stored in the dark at -20 °C until analysis on-board the ship. Samples were then extracted with

90% acetone in the dark (4 °C, 24 h) and measured using a 10AU fluorometer fitted with a red-sensitive photomultiplier tube (Turner Designs). Sample signals were calibrated using a chlorophyll *a* standard (Sigma) and were corrected for phaeopigments by accounting for the fluorescence of extracts before and after acidification with 0.003 M HCl (*36*).

Cell counts

Seawater samples were preserved for flow cytometry analyses by pre-filtering through a 40 µm mesh, fixing with 0.5% glutaraldehyde (final concentration), flash freezing in liquid nitrogen, and storing at -80 °C until analysis. Microbial cell counts were conducted on a Guava EasyCyte HT flow cytometer (Millipore Sigma) with blue laser (488 nm) calibrated with instrument-specific beads. Samples were analyzed at a low flow rate (0.24 mL s^{-1}) for 3 min. Phytoplankton groups were counted based on size-dependent forward scatter vs. red chlorophyll fluorescence at 675 nm (eukaryotes) or orange phycoerythrin fluorescence at 585 nm (*Synechococcus*). Size classes of eukaryotic phytoplankton were further distinguished based on forward scatter (pico-, nano- and large eukaryotes up to 40 µm). To enumerate bacteria, samples were diluted (1:100) with autoclaved filtered seawater (0.1 µm), stained with SYBR Green I (Invitrogen) according to the manufacturer's instructions in a 96-well plate in the dark at room temperature for 20 min. Bacterial cells were counted based on diagnostic forward scatter vs. SYBR green fluorescence at 530 nm.

Soluble reactive phosphorus (SRP)

Select samples for soluble reactive phosphorus (SRP) were analyzed with the following manual method. Briefly, seawater was filtered through 25 mm GF/F glass fiber filters with nominal pore size of 0.7 µm (Whatman), which were previously combusted at 550 °C overnight, then acid-washed with 10% HCl overnight, and rinsed three times with Milli-Q water. The filtrate was collected in 60 mL acid-washed high density polyethylene bottles and frozen at -20 °C until analysis. SRP concentrations were measured as phosphomolybdate heteropoly acid using a standard colorimetric method (*7*) on a Cary 60 UV-Vis Spectrophotometer (Agilent) using a 4 cm glass spectrophotometry cell on triplicate subsamples. The detection limit, defined as three times the standard deviation of replicate blank measurements, was 13 nmol L^{-1} SRP. Data obtained by this method included station 1 (15 m), station 2 (20 m), station 3 (40 m), and station 4 (140 m; **Table 1**), and SRP depth profiles used to calculate DOP (**Fig. S3**).

Dissolved organic phosphorus (DOP)

Dissolved organic phosphorus (DOP) was defined as the difference between total dissolved phosphorus (TDP) and soluble reactive phosphorus (DOP = TDP-SRP). SRP values were obtained using the manual method described above. Samples for TDP were filtered through 25 mm GF/F glass fiber filters with nominal pore size of 0.7 µm (Whatman), which were previously combusted at 550 °C overnight, then acid-washed with 10% HCl overnight, and rinsed three times with Milli-Q water. The filtrate was collected in 60 mL acid-washed high density polyethylene bottles and frozen at -20 °C until analysis. TDP concentrations were determined by the ash/hydrolysis method (*8*), in which 20 mL sample volume was treated with 0.4 mL of 0.17 M $MgSO_4$ in an acid-cleaned, muffled glass jar and dried without cap at 95 °C overnight. Dried samples were ashed at 550 °C for 2 hours before cooling, acidifying with 3 mL 0.75 M HCl, and heating with cap at 80 °C for 20 min. Samples were diluted to a total volume of 20 mL H_2O and heated at 80 °C for another 10 min. Once at room temperature, samples were quantified using the manual method for SRP described above. Due to lack of direct measurement, the DOP value at station 3 was modeled using

Ocean Data View according to the 'Estimating Z-Values at Arbitrary X/Y Points' section of the ODV HowTo, Version 5, February 3 2024 (*37*). A dataset of DOP concentrations at different depths along the survey track of P2107 in the CCE was used as isosurface variable for modeling (**Fig. S3b**). Desired values were estimated using the gridded field DIVA gridding procedure.

Dissolved inorganic nutrients

Surface concentrations of dissolved inorganic nutrients (ammonium, nitrate, nitrite, silicate, and phosphate) for the CCE-LTER process cruise P2107 were acquired following California Cooperative Oceanic Fisheries Investigations (CalCOFI) protocols (*38*). Samples were dispensed into 30 mL acid-cleaned polypropylene screw-capped centrifuge tubes rinsed three times with sample before filling, and stored at -20 °C before analysis. Concentrations were measured using a colorimetric assay on a SEAL Analytical continuous segmented flow autoanalyzer 3 (AA3) at the Oceanographic Data Facility (ODF) Chemistry Laboratory, Scripps Institution of Oceanography. Data obtained by this method were ambient environmental surface concentrations (~2 m) throughout the P2107 survey transect (**Fig. 1**), and macronutrient depth profiles at stations 1-4 (**Fig. S2**). Silica excess (Si_{ex}) values were calculated from inorganic nitrate and silicate data as described previously (*29*).

Alkaline phosphatase activity (APA)

Alkaline phosphatase activity (APA) assays were carried out in a black, flat-bottom 96-well plate (200 µL per well) using 190 µL sample volume and 10 µL of the fluorogenic probe 4-methylumbelliferyl phosphate (MUF-P, Millipore Sigma). Reactions were initiated by addition of MUF-P (400 µM stock solution in H_2O; 20 µM final concentration), mixed, and incubated at room temperature. Degradation of MUF-P to 4-methylumbelliferone (MUF) with concomitant release of PO_4^{3-} was analyzed by a standard fluorescence technique (*5*) (excitation: 359 nm, emission: 449 nm) every 5-10 min for 3-24 h using a SpectraMax M3 multimode microplate reader (Molecular Devices). For control reactions, trace metal clean seawater from each station was filtered in-line with a 0.2 µm Acropak-200 filter (VWR international) and stored at -20 °C prior to assays. Background MUF-P autohydrolysis were boiled (99 °C, 20 min), amended with nutrients (see *Field incubations*), reacted with 20 µM MUF-P, and subtracted from the experimental APA rates. Data were corrected for background fluorescence present in unamended controls and calibrated with a multipoint standard curve of MUF (10–500 nmol L^{-1}) prepared in 0.2 µm-filtered seawater. MUF-P hydrolysis rates were calculated as the slope of the best fit line ($R^2 \geq 0.98$) of MUF concentration versus time. A final concentration of 20 µM MUF-P was assumed to be rate-saturating based on preliminary experiments with natural samples. Thus, the rates of APA reported herein represent maximum extracellular hydrolysis rates, consistent with previous investigations of APA (*10*).

Metatranscriptomics

Samples for eukaryotic mRNA were collected by filtering 3 L or 1 L of seawater from Niskin bottles (ambient condition) or incubation bottles, respectively, through a 0.22 µm Sterivex-GP filter (Cat. no. SVGP01050, Millipore). The filter was immediately sealed with both a luer-lock plug, previously cleaned with 1.2 mol L^{-1} HCl then Milli-Q, and Hemato-Seal™ tube sealant, wrapped in aluminum foil, and flash frozen in liquid nitrogen. RNA was extracted using the NucleoMag RNA extraction kit (Machery-Nagel) on an Eppendorf epMotion 5075t, as described previously (*39*). RNA quality was assessed using an Agilent 2200 TapeStation (RNA ScreenTape),

and quantified using the Quant-iT™ Ribogreen® RNA assay kit. Poly-A selected libraries were constructed with the KAPA mRNA HyperPrep Kit, and sequencing was performed at the UC Davis Genome Center on an Illumina NovaSeq 6000.
Raw reads were quality trimmed with trimmomatic v0.39 (*40*) and evaluated with FastQC v0.12.1 and MultiQC v1.9.dev0 (*41*). Ribosomal RNA reads were also removed with SortMeRNA v4.3.6. The remaining reads were then assembled into contigs using both individual samples with rnaSPAdes v3.13.0 (*42*) and replicate samples with MEGAHIT v1.2.9 using the meta-large preset (*43*). Assemblies were then combined and deduplicated with dedupe.sh from BBMap v38.18. From the combined assembly, proteins were predicted with GenemarkS-T (*44*), which were then clustered based on 98% similarity with MMSeqs2 v13-45111 and filtered for rRNA with SortMeRNA again.
Reads were mapped to the predicted proteins with Bowtie2 v2.5.1 in local alignment mode (*45*). Only reads with a MAPQ score ≥ 8 were retained. Taxonomic annotation of predicted proteins was performed with DIAMOND (v2.1.8) BLASTP searches against PhyloDB v1.076 (*46, 47*) with an E-value cutoff of 10^{-5}, minimum query coverage of 60%, and alignment sores in the top 95%. To avoid mis-annotations from contamination in the reference database, final taxonomic assignment was based on the Lineage Probability Index from the BLASTP hits with the aforementioned cutoffs (*48, 49*). For functional annotation, DIAMOND BLASTP searches were performed against the Kyoto Encyclopedia of Genes and Genomes (KEGG; Release 94.1) (*48, 50*). KEGG Ortholog (KO) assignment was performed with KOfamKOALA which utilizes hmmsearch against KOfam, an HMM database of KOs (*51*). Genes without KOs were manually annotated based on their KEGG gene annotation as listed in Supplementary **Tables S1-S5**.
Relative abundances of eukaryotic transcripts were assessed by dividing the total number of transcripts per million (TPM) for each gene of interest by the total number of eukaryotic TPM.

Statistical analyses
Statistical analyses of chlorophyll, cell counts, and APA were performed in JMP Pro (15.2.0) using repeated-measures ANOVA followed by Tukey's Honest significant difference (HSD) test. Statistical analyses of mRNA (fold-changes) were performed in R using the DESeq2 v1.42.1 Wald test adjusted for multiple testing via the Benjamini and Hochberg method (*52*). p-values and adjusted p-values <0.05 were considered significant.

Results

Chlorophyll* a *and phytoplankton abundance
The cruise track followed an onshore-to-offshore gradient in productivity from coastal upwelling in the CCE toward the North Pacific subtropical gyre (**Fig. 1a, Table 1**). Inshore, station 1 featured high chlorophyll *a* (Chl *a*) and phytoplankton cell concentrations, which indicated the onset of a bloom. Quasi-Lagrangian tracking of this discrete water parcel showed that Chl *a* doubled while phytoplankton cell concentration remained similar at station 2. Station 3, in the transition zone, and station 4, located at the border of the oligotrophic North Pacific subtropical Gyre, featured much lower biomass compared to the two coastal upwelling stations 1-2. Similarly, the chlorophyll maximum deepened going from onshore to offshore (**Fig. S1**). During the June 2022 cruise SR2003, located south of P2107 in a non-upwelling area, ambient cell concentrations averaged 4,920 cells mL^{-1}, comparable to phytoplankton abundances between P2107 stations 3 and 4.

Dissolved macronutrients

At the surface (~2 m), The upwelling event at station 1 injected more than 1 μM phosphate into the euphotic zone (**Fig. 1a**). Surface (~2 m) phosphate was quickly removed further offshore until reaching values between 0.29-0.52 μM (**Fig. 1a**). Phosphate was also measured at depth in waters used for experimental on-deck incubations. Station 1 at 15 m showed a concentration of 0.69 μM, which increased to 1.07 μM at station 2 at 20 m (**Table 1**). The transition station 3 at 40 m and offshore station 4 at 140 m featured 0.72 and 0.77 μM phosphate, respectively (**Figs. S2-3**). At the surface (~2 m), nitrate concentrations generally followed the trend of phosphate, except for depletion below the limit of detection at offshore station 4 (**Fig. S2**). Nitrate was considered replete (> 7 μM) at the incubation sampling depths of stations 1-4, but decreased slightly from onshore to offshore (**Table 1**). Dissolved inorganic N to P ratios fell below the Redfield ratio of 16 (*53*) at stations 2-4 (N:P = 10.58-11.44), and above Redfield at station 1 (N:P = 19.54; **Table 1**). Dissolved organic phosphorus (DOP) made up a maximum of 98% of the ambient total dissolved phosphorus (TDP) pool at the surface (~2 m) of the cruise transect and between 29-64% at depths of stations 1-4 (**Table 1**; **Fig. S3**).

Alkaline Phosphatase Activity (APA)

Despite the prevailing phosphate-replete (> 0.5 μM) environment, alkaline phosphatase activity (APA) was measurable at all stations (**Fig. 1b**). Ambient rates of APA were measured at the incubation sample depths (**Table 1**) and rose from 26.0 nM day^{-1} at station 1 to 39.9 nM day^{-1} at station 2, then declined to 13.7 and 8.2 nM day^{-1} at stations 3 and 4, respectively (**Fig. S4**). When normalized to Chl *a*, specific APA increased 4-fold along the on- to offshore continuum, from ~0.5 nmol μg^{-1} hr^{-1} in costal regimes (stations 1-2) to 1.75 at station 3 and 3.48 at station 4 (**Table 1**). This trend was even more pronounced for APA normalized to cell concentration, which enhanced 14-fold from station 1 to station 4 (**Fig. S4**). No correlation was found between APA, phosphate concentrations, or N:P ratios (**Fig. S5**).

Eukaryotic community composition

Dinoflagellates (Dinophyta) constituted the main eukaryotic phytoplankton class at stations 1-4 (**Fig. 1c**) and mostly contained the harmful algal bloom-forming species *Alexandrinum*, *Ceratium* and *Kareniaceae* (**Fig. S6**). Prymnesiophyceae, especially *Emiliania* and *Phaeocystis* spp., were the second most abundant eukaryotes, followed by diatoms (Bacillariophyta), the green algae class Mamiellophyceae, and *Pelagomonas*, a small picoeukaryote that dominates deep chlorophyll maxima in this region (*54*). Besides dinoflagellates and Prymnesiophyceae, diatoms were more prevalent at stations 1-2, Mamiellophyceae and *Pelagomonas* at station 3, and *Pelagomonas* at station 4 (**Fig. 1c**). Coastal diatoms were predominantly from the centric lineage (65-73%), including the dominant chain-forming *Chaetoceros, Thalassiosira,* and *Pseudo-nitzschia*, while the percentage of pennate diatoms increased in transition and offshore zones (42-47%; **Fig. S7**). Mamiellophyceae consisted majorly of *Bathycoccus*, *Ostreococcus*, and *Micromonas* (**Fig. S6**). Other large eukaryotic contributors include ciliates (3.4-6.1%), cryptophytes (3.2-4.6%), other stramenopiles (8.5-10.5%) and rhizaria (0.6-0.7%). Overall, the eukaryotic community composition differed substantially among the coastal (stations 1-2) and offshore (stations 3-4) locations (**Fig. S8**).

Functional gene expression

To assess the nutritional status of ambient plankton assemblages, relative transcript abundances of established nutrient stress biomarkers were tracked from onshore to offshore. The N stress genes for nitrate assimilation (NRT2, NR, *nirA*) (*55*) and alternative N acquisition such as urea uptake or amino acid catabolism (DUR3, *glnA*) (*56, 57*) were overrepresented at stations 1 and 4 (**Fig. 2a)**. The iron starvation induced proteins ISIP1-3 (*58-60*), flavodoxin *fldA* (*61*), and the photosystem antenna *psbC* (*62*) peaked at stations 2 and 3, albeit with slight variances in the extent of accumulation (**Fig. 2b**). Enriched transcripts for the Zn/Co responsive proteins ZCRPA/B as well as potential divalent Zn/Co transporters of the ZIP family were found at station 2 (**Fig. 2d**) (*55, 63, 64*). Molecular markers for phosphate stress, i.e. the high-affinity Pi transporters *pstS* (*55, 65*) and *SLC34A* (*66*), the low-Pi induced AP isoform *phoA* (*10*), and *SQD1*, which converts phospholipids to sulfolipids under Pi scarcity (*67*), show a general trend of decreasing stress from station 1 to 4, with the exception of *phoA* at station 1 (**Fig. 2c**).

A multitude of DOP utilization signatures was present throughout the CCE (**Fig. 2e**), including genes involved in the utilization of all major DOP bond classes: P-esters, P-anhydrides, and phosphonates. However, many Kyoto Encyclopedia of Genes and Genomes (KEGG) orthologies (KOs), which are commonly used for functional metatranscriptome annotations (*68*), did not capture several marine microbial APs. These genes fell into two categories (**Tables S3-4**): (1) those that could be assigned to an existing KO based on literature references or BLASTP search, and (2) those that could not. In particular, the latter case included atypical APs (AP_{aty}), e.g. atypical $PhoA_{aty}$ of *Emiliania huxleyi* (*69, 70*); and phosphodiesterases. Hence, we compiled AP_{aty} with 12 published and manually annotated homologs of atypical AP sequences stemming from stramenopiles, prymnesiophytes, and green algae (**Table S3**). Two categories of uncharacterized P-diesterases (PDEs), containing 20 previously reported and manually assigned genes from diatoms, hacrobia, and green algae, were created in a similar manner (**Table S4**). The first PDE category, Phospholipase C (PLC)-like PDEs (3 genes), are involved in the degradation of phosphoinositides, while 'other' PDEs (17 genes) represent extracellular, dimetal-containing P-diesterases.

Other PDEs ('other') constituted with up to 33% the largest fraction of genes encoding DOP-degrading proteins observed in the study area, followed by pyrophosphatases (*ppa*), NUDIX hydrolases, PLC-type PDEs, *phoD* and *ugqQ* (**Fig. 2f**). Atypical AP isoforms (AP_{aty}) were within 4-5% of DOP-targeting genes comparable to *phoA* (2-9%) and *phoX* (1-4%). All genes had broad taxonomic representation, with many PDEs ('PLC'-type and 'other') attributed to prymnesiophytes, *ppa* to dinoflagellates, *ugpQ* to diatoms (**Fig. S9**).

Responsible for the assimilation of P-monoesters, AP_{aty} was highest at stations 1-2, *phoA* and *phoD* at station 2, *phoX* and the *E. huxleyi*-type AP EHAP1 most abundant at station 4, and the high-affinity phosphatase *psip1* (*71*) enriched at station 3 (**Fig. 2e**). 'Other' PDEs dominated at station 1, *ugpQ* at station 2, and PLC-type PDEs and P-triesterases (PTER) at station 4. Genes involved in P-anhydride metabolism, i.e. *ppa*, exopolyphosphatses (*ppx*), and NUDIX hydrolases, occurred from stations 1-3, whereas the phosphonate-degrading oxygenases *phnYZ* seemed restricted to the offshore station 4.

Table 1: *In situ* environmental conditions at stations 1-4. Error values represent one standard error of the mean, $n = 3$.

Station	Condition	Depth (m)	PO_4^{3-} (μM)	NO_3^- (μM)	DIN/ DIP	DOP/ TDP (%)	APA (nmol μg^{-1} hr^{-1})	Chl *a* (μg/L)	Phytoplankton (cells/mL)
1	New Upwelling	15	0.69 ±0.09	13.52 ±0.17	19.54	39.7	0.51 ±0.09	2.11 ±0.21	38,300 ±1,350
2	Aged Upwelling	20	1.07 ±0.16	12.11 ±1.18	11.34	54.2	0.53 ±0.06	4.38 ±0.30	32,700 ±1,550
3	Transition	40	0.72 ±0.02	7.56 ±0.05	10.58	29.2	1.75 ±0.03	0.45 ±0.03	19,680 ±510
4	Offshore	140	0.77 ±0.13	8.80 ±0.20	11.44	63.6	3.48 ±0.46	0.10 ±0.002	910 ±295

Nutrient-addition incubations

To investigate the regulation of microbial growth, community structure, and P nutrition under different nutrient stress regimes within the CCE, shipboard bottle incubations were performed at stations 1-4 with addition of the potentially limiting nutrients Fe and N. Eukaryotic community metatranscriptomics analyses were conducted from bottle incubations at stations 2 and 4.

Chlorophyll *a* and phytoplankton abundance

After an incubation time of 48 hours, phytoplankton growth by Chl *a* increased at coastal stations 1 and 2 following Fe additions (Fe and FeN; **Fig. 3a,b**). In contrast, at the offshore station 4, Chl *a* was stimulated following N additions (**Fig. 3c**). The growth response to N was mirrored by a significant increase in phytoplankton cell abundance offshore (station 4), while stations 1 and 2 did not show significant changes in cell counts (**Fig. 3d-f**). No significant responses of phytoplankton growth to nutrient additions were detected at station 3 (**Fig. 3g**). For SR2003, phytoplankton cell counts were significantly higher within Zn or Fe-amendments, with or without N (**Fig. S10**).

Alkaline phosphatase activity (APA)

In the course of shipboard incubations, Chl *a*-normalized APA increased significantly upon N additions at coastal stations 1 and 2 (N vs. Ctrl, $p < 0.05$, **Fig. 3a,b**), and upon Fe amendments at the offshore station 4 (FeN vs. Ctrl, $p < 0.05$; Fe vs. Ctrl, $p = 0.066$, **Fig. 3c**). Cell-normalized APA also showed a significant stimulation by N at station 2 (N and FeN vs. Ctrl, $p < 0.05$, **Fig. 3d,e**), and by Fe at station 4 (Fe and FeN vs. Ctrl, $p < 0.05$, **Fig. 3f**). At the transition station 3, cell-normalized APA responded positively to Fe treatments (Fe and FeN vs. Ctrl, $p < 0.05$, **Fig. 3g**). For SR2003, specific APA exhibited no significant changes when normalized to phytoplankton cell counts (**Fig. S10**), but rose significantly upon Zn, Fe+N, or Zn+N additions when normalized to counts of all microorganisms (**Fig. 3h**).

Eukaryotic community composition

For incubation experiments at station 2, Fe treatments (+Fe, +FeN) caused a 7-10% increase in the relative abundance of diatoms, and a 6-8% decline in dinoflagellates (**Fig. 4a**). Upon N additions (+N), the presence of dinoflagellates increased by 11%, while diatoms and Prymnesiophyceae diminished slightly. Mamiellophyceae, *Pelagomonas*, and other eukaryotes exhibited only small changes (< 2%) at station 2.

At station 4, *Pelagomonas* was the dominant community member in incubation bottles. Fe amendments (+Fe, +FeN) resulted in a larger contribution of diatoms (2-4%), dinoflagellates (4-12%), and other eukaryotes (2-3%), whereas *Pelagomonas* became 20% less abundant (**Fig. 4b**). Added N had a negligible effect on community composition (< 2%). Mamiellophyceae and Prymnesiophyceae exhibited only small changes (< 2%) at station 4.
Overall, the transcriptional profile of the eukaryotic community was distinct between stations and showed clear differences among treatments, with larger variance between Fe-containing treatments (+Fe, +FeN) versus +N or Ctrl (**Fig. 4c**).

Functional gene expression

Metatranscriptomes were compared to elucidate taxonomic changes associated with growth and APA responses to nutrient additions. Eukaryotic community transcripts showed diminished Fe stress markers upon increasing Fe availability at station 2 (+Fe and +FeN; **Fig. S11**), and diminished N stress markers upon increasing N availability at station 4 (+N and +FeN; **Fig. S11**). In addition, amendments with one nutrient caused certain stress biomarkers for other nutrients to increase above the control. For example, several molecular markers for P stress were elevated in +Fe incubations (*pstS, SLC34A*, *SQD1*), as well as +N incubations (*SLC34A*, *phoA*) at station 2 (**Fig. S11**).
At the upwelling station 2, N stimulated microbial community APA, and atypical AP_{aty} transcripts were the most prevalent phosphatase among the genes encoding DOP hydrolases for this treatment (34%; **Fig. S12**). On a whole community level, the relative abundances of AP_{aty} and *phoA* genes increased in +N compared to the control (**Fig. 5a**), with AP_{aty} displaying a significant fold-change ($P < 0.001$; **Fig. S13**). On a taxonomic level, diatoms showed a significant overrepresentation AP_{aty} and *phoA* in +N samples versus the control (**Figs. 5c**), as well as the P-stress markers *pstS* and *SLC34A* (**Figs. S14-15**). Although other DOP-degrading genes were less abundant than AP_{aty} and *phoA*, several of them responded significantly to +N, including *phnY* and *ppa* in *Pelagomonas,* 5'-NT and PLC-type PDE in mamiellophytes, and *ugpQ* and NUDIX in prymnesiophytes (**Fig. 5c**), yet these organisms did not display elevated P stress markers (**Fig. S14**). Similar transcriptional responses were observed in the +FeN treatment (e.g., significant increases in DOP hydrolases for all taxa in +FeN vs. Ctrl; **Fig. S15**).
In contrast, at the offshore station 4, Fe stimulated microbial community APA, and "other" PDEs were the dominant phosphatases among the genes encoding DOP hydrolases for this treatment (64-72%; **Fig. S12**). On a whole community level, the relative abundances of *ugpQ* and "other" PDEs were elevated under +Fe and +FeN (**Fig. 5b**), respectively, compared to the control. Within dominant phytoplankton groups, +FeN additions coincided with significant overrepresentation of "other" PDEs in diatoms, dinoflagellates, and mamiellophytes (**Fig. 5d**), as well as NUDIX in mamiellophytes (**Fig. S15**). In +Fe treated samples, no previously considered phosphatase gene showed significant fold-changes within major taxa. However, +Fe induced a significant spike in P stress markers within diatoms (*SLC34A*; **Fig. S14-15**) alongside the NAD^+ kinase *ppnK* (**Fig. 5d**), which phosphorylates NAD under consumption of P-anhydrides. At the same time, diatoms downregulated their gene transcription of Fe-harboring *phoD* and *phoX* (**Fig. S15**).

Discussion

Secondary P stress contributes to APA in a nutrient-rich upwelling region.

The goal of this study was to examine the utilization of DOP along variations in nutrient availability, including a gradient from coastal upwelling waters to the open ocean, and bottle incubation experiments. Typically, the activity of APs, especially PhoA, is induced in response to P depletion and used as an indicator for nutritional P stress (*10*), a distinct metabolic state in cells experiencing low phosphate (Pi/PO_4^{3-}) supply. The CCE was characterized as relatively P-replete by high ambient P concentrations of >0.5 μM, N;P ratios generally below 16, and primary limitation by either Fe or N (**Tables 1-2**). Despite this P status, we found measurable APA rates as well as DOP utilization genes across all stations.

APA in this study is with 8-82 nmol day^{-1} comparable to or slightly higher than prior observations in the North Pacific (*10, 72*), other Pi-rich eastern boundary upwelling systems (*3, 73*), and background APA levels in the subtropical ocean where Pi is not scarce (*10*). Different explanations for 'basal' or 'background' APA in high Pi regions have been invoked, including constitutive and Pi-insensitive phosphatases of certain eukaryotic phytoplankton groups (*3*) or heterotrophic bacteria (*74-76*), i.e. PafA (*75*), 5'-NTs (*77*), as well as the regulation of PhoX by DOP rather than Pi availability (upregulated >90 nM DOP) (*78*). Indeed, several studies in Pacific gyres show biomass-normalized APA to be constitutive across natural or experimental phosphate gradients (*10, 13, 79*).

At least part of the explanation for APA in the CCE includes phytoplankton community members that spatiotemporally experience a certain degree of P stress, despite high Pi concentrations, as reported for bloom and bust cycles (*5*). Our results from this study analyses indicate multistressor landscapes of primary Fe limitation and additional N, P and Zn/Co stress during late upwelling (station 2), and primary N limitation and additional Fe and P stress offshore (station 4; **Table 2**). First, the low ambient N:P ratios (**Table 1**) do not necessary reflect an excess or replete P status, since flexible microbial P stoichiometries due to metabolic plasticity can sometimes lead to non-Redfield patterns with diminished ratios in eutrophic and elevated ratios in oligotrophic areas, and a below-Redfield global average (*2*). Second, secondary P stress is supported by genetic nutrient stress indicators in ambient and incubation conditions implying a choreography of multiple stressors including P. At station 1, overrepresented *pstS*, *SLC34A*, and *SQD1* transcripts (**Fig. 2**), together with an above N:P ratio above 19 (**Table 1**), suggest some degree of P stress. Under incubation conditions, alleviation of proximal nutrient shortages often caused other stress biomarkers to spike (**Fig. S10**), hinting at underlying multifaceted serial or potentially co-limitation scenarios, which were often specific to taxonomic groups (**Figs. S14**). For example, offshore diatoms displayed signals for Fe-N co-limitation (i.e., significant decreases of both Fe and N stress markers under +FeN), and transcribed significantly more P stress biomarkers when either one or both of these nutrients were added (**Fig. S14**). Altogether, secondary P stress in one or more phytoplankton groups likely contributes to DOP cycling in the CCE (**Table 1**).

Community responses to nutrient additions and underlying molecular drivers.

During nutrient addition incubations, the natural mixed phytoplankton assemblage displayed contrasting responses in microbial growth and APA to Fe and N amendments. The basis of Fe-promoted APA is thought to be an increased supply of reactive cofactors for Fe-dependent DOP hydrolases (*2*), whereas N-promoted APA is caused by a rise in macronutrient Redfield ratios

toward P shortages (*13*). Here, metatranscriptomics was applied to clarify the molecular and taxonomic drivers of these potential ecophysiological changes.

Station 2

At station 2 with aged upwelling conditions, Fe-stress biomarkers and community incubations indicated proximal Fe-limitation of phytoplankton growth, as observed previously for similar habitats in the CCE (*80*). This growth response is likely driven by chlorophyll-rich, large diatoms due to several indicators. First, community composition inferred from poly(A)-selected metatranscriptomes demonstrates that diatom abundance increased in +Fe and +FeN treated samples (**Fig. 4a**). Second, negative silica excess values (Si_{ex}), which serve as indicator for Fe-limitation in diatoms due to their silicic acid-containing frustules (*29*), were present at coastal stations 1-2 (**Fig. S2**). Third, ambient and incubation trends in Chl *a* pigments were not mirrored using cell enumeration (**Table 1, Fig. 3b,e**). This is consistent with the dominance of larger chain-forming genera such and *Pseudo-nitzschia* at station 2, since particles >40 µm needed to be removed before flow cytometry analysis (see *Materials and Methods*).

At this station, microbial community APA increased in response to N additions. AP_{aty} transcripts in diatoms likely dictated bulk APA due to their large contribution to the phosphatase pool (28%) and 2.2-fold upregulation in the +N treatment (**Fig. 5c**), with additional contributions from other proteins. The overrepresentation of AP_{aty}, *phoA*, and P stress biomarkers in diatoms under +N suggests that Fe-limited coastal diatoms in the CCE had transiently unfulfilled P demands toward the end of the observed bloom. While N-additions enhanced APA, we did not observe increases in Chl *a*, diatom community contribution, or larger eukaryote cell abundance. One potential explanation for this decoupling is that a biologically constraining nutrient other than P (here: Fe) is still stifling growth, as has been observed previously for N-P co-limited natural communities in the North Atlantic (*11*). Another possible reason is that net Chl *a* and bulk APA are driven by different diatom genera, i.e. *Chatoceros* and *Pseudo-nitzschia* vs. *Thalassiosira* and other diatoms (**Fig. S6**). The nutrient combination of +FeN did not lead to enhanced APA likely due to Fe-induced changes in microbial physiology (alleviation of primary Fe-limitation) and community composition (**Figs. 4a, S16**).

Station 4

At station 4 within the offshore zone, N-stress biomarkers and community incubations indicated that N was the primary limiting nutrient for phytoplankton growth. This growth response is likely driven by shifts in the whole phytoplankton community. Metatranscriptomics revealed a larger proportional contribution by *Pelagomonas* in Ctrl and +N samples (**Fig. 4b**), which was contested by dinoflagellates and diatoms in +Fe and +FeN samples. Consequently, we hypothesize that N was incorporated into total biomass over the entire photosynthetic assemblage, which is also reflected in elevated phytoplankton cell counts (**Fig. S10**). Growth in +FeN likely differed from +N due to community composition changes associated with alleviating underlying Fe stress of several taxa (diatoms, prymnesiophyceae, mamiellophyceae, **Fig. S14**). Both chlorophyll *a* as well as cell counts aligned due to the absence of large chain formers (**Fig. 4c,f**).

At this station, microbial community APA increased in response to Fe additions. No P-monoesterase increased significantly in +Fe or +FeN samples; however, biochemical experiments demonstrate that several promiscuitive PDEs of terrestrial bacteria also target P-monoesters (*81, 82*). Hence, elevated APA upon +FeN addition can be ascribed to a significant overrepresentation of PDEs in dinoflagellates, diatoms, and mamiellophyceae, resulting in a 12% relative increase in

"other" PDE transcript abundance versus the control (**Fig. 5b**). The metal cofactors for these extracellular enzymes are poorly constrained, but might involve binuclear Fe, Zn or Mn centers (*83*).

In +Fe samples, the relative abundance of *ugpQ* doubled relative to the control, but was not accompanied by significant fold-changes for any taxa. Constituting 1.5-3%, *ugpQ* was the 2nd most abundant phosphatase after PDE (other). In addition, we noticed significantly higher diatom *ppnK* transcription, a NAD^+ kinase that consumes P-anhydrides, suggesting that APA increased due to higher diatom P demand for NADP production. Indeed, the NADP requirement of Fe-stressed diatoms is reported to increase due to resource allocation toward carbon fixation after replenishing Fe (*62*). This allocation includes routing Fe toward the biogenesis of Fe-S clusters, which we also observed (**Table S6**), and explains the significant decrease in Fe-demanding *phoD* and *phoX* (**Fig. S15**). A complementary explanation for increased P/NADP demand is the mitigation of oxidative stress and metal homeostasis under sudden Fe influx (*84, 85*). We thus hypothesize that elevated APA under +Fe stems from proliferating diatoms' enhanced P requirements addressed by *ppnK* (4th most abundant DOP-targeting gene offshore), in combination with *ugpQ*.

Overall, diatoms in this study showed the most significant changes in their P metabolism, and were major drivers of biogeochemical (APA) and physiological (Chl *a*) community responses to nutrient variations (**Table 2**). In contrast, more abundant dinoflagellates and *Pelagomonas* exhibited less significant changes in their P transcriptome and minorly influenced observations. Our conclusion that diatoms were key taxa responsible for observed APA trends is consistent with a study at the Oregon coast, where diatom APs mimicked the observed in *situ* APA rates more than other taxa including dinoflagellates, especially under N-induced P stress (*3*). This driving role is also reflected in diatoms' normalized gene expression of AP_{aty}, *phoA*, *phoD*, *phoX*, *ppa* and *ugpQ* being the highest among all taxa (**Fig. S17**).

Table 2. Main drivers of microbial responses within nutrient addition incubations.

Station	Growth-Controlling Nutrient	Additional Nutrient Stressors	Growth-Driving Taxa	APA-Controlling Nutrient	APA-Driving Taxa	APA-Driving Proteins	DOP Classes Targeted
2 (Aged)	Fe	N, P, Zn/Co	Diatoms	N	Diatoms	AP_{aty}, *phoA*, NUDIX, *ppa*	P-monoesters P-anhydrides
4 (Offshore)	N	Fe, P	All	Fe	All	PDE (other), *ugpQ*, *ppnK*	P-diesters P-anhydrides Phosphonates

Functional diversity among microbial taxa and implications for marine ecosystem measurements.

This study has shown that eukaryotic primary producers between the California Current and the oligotrophic North Pacific subtropical gyre experience various degrees of P stress, to which they react with molecular DOP acquisition strategies distinct between taxonomic clades.

The manually curated gene compilations AP_{aty} and PDE (other), which were not included in KOs, were highly abundant among all microbial phosphatases (**Fig. 2f**), and their expression was very responsive to changing environmental conditions (**Table S7**). PDE (other) in particular was transcribed among the top 1% of the coding metatranscriptome pool in offshore incubations at station 4 (**Table S7**). AP_{aty} genes were transcribed among the top 3% of all eukaryotic genes in coastal incubations at station 2. For comparison, ISIPs were transcribed in the top 0.1-2% under

Fe-limitation (station 2) and in the top 2-39% when Fe was not limiting (station 4), making PDE (other) and AP_{aty} comparable to highly prevalent stress biomarkers, which can reach protein concentrations of up to 2.5 pM (*65*). More importantly, both exceeded *phoA*, *phoD* and *phoX* at all stations, which only ranked in the top 14-26% expressed genes under equivalent conditions (**Table S7**). Given that metatranscriptomics annotation often relies on KEGG or similar databases for functional assignments (*68*), the results from AP_{aty} and PDE (other) illustrate that major drivers might not be present in these reference databases and missing in studies that solely rely on existing orthologies. This also illustrates the need for more functional annotation of marine eukaryotic genes and their incorporation in routine 'omics analyses.

Normalized expression of transcripts and their responses to natural (ambient) or artificial (added) changes in nutrient availability varied greatly between community members, highlighting the tailored occupation of different metabolic niches (**Fig. S15, Table S7**). In general, diatoms, dinoflagellates, and prymnesiophytes exhibited the widest functional diversity and transcribed all phosphatases tested (**Table S7**). However, diatom phosphatases exhibited the most significant changes to nutrient additions in our incubation bioassays (**Fig. S15**). In comparison, the more streamlined green algae (*86*) and *Pelagomonas (87)* lacked several P-esterases and phosphonatases (**Table S7**). Notably, other PDEs as well as *ppa* were most responsive overall to environmental stimuli. Validating previous assumptions, *phoD, phoX,* and *psip1* in particular changed upon Fe variations, while *phoA* and PDE (other) were activated by N (**Fig. S15**).

We anticipate DOP cycling in the CCE to encompass further mechanisms, including different classes of DOP-targeting proteins, additional environmental regulators, and other involved organisms including cyanobacteria and heterotrophic bacteria. Regarding different proteins, certain enzymatic responses to nutrient availabilities are not detected using the MUF-P assay we applied here, which predominantly targets P-monoesterases. For instance, the phosphonate-degrading protein *phnY* was significantly upregulated in *Pelagomonas* for both +N and +FeN treatments at station 2 (**Fig. S15**), indicating that eukaryotic C-P lyase expression might also be activated to combat P stress as reported for bacterioplankton (*23, 88*), and emphasizing the need to apply different field bioassays to assess various molecular stress mechanisms (*89*).

Regarding environmental regulators, biomarkers for Zn and Co stress were elevated at location 2, along with overrepresented transcripts of AP_{aty}, *phoA*, *phoD*, and *ugpQ* (**Fig. 2**). Since Zn-limitation of APA, presumably via Zn/Co-harboring P-esterases and other hydrolases (*2*), has been observed in the field (*10*), it is possible that Zn/Co stress contributes to the changes in APA and transcription observed here. Results from a second research expedition (SR2003) in the southern CCE corroborate this assumption, where phytoplankton growth was found to be proximally co-limited by Zn and Fe (**Fig. S10**). Here, APA was significantly stimulated by Zn when normalized to total microorganism cell counts, including heterotrophic bacteria (**Fig. 3h**). This observation confirms Zn shortages in the CCE to influence microbial growth and P acquisition, although likely on the basis of divergent mechanisms. In comparison, Co additions had no effect (**Fig. S10**).

Lastly, further mechanisms governing *in situ* DOP hydrolysis rates may involve organisms other than eukaryotic phytoplankton, as activity has been reported for cyanobacteria (*21*), heterotrophic bacteria (*74-76*), or zooplankton (*90*). Our incubation experiments lacked organic carbon amendments and were designed, on that basis, to primarily stimulate phytoplankton rather than heterotrophs. Indeed, no trends were found for using cell enumerations of heterotrophic bacteria for these incubations (data not shown). Furthermore, our transcriptomic analysis did not investigate prokaryotic gene expression. *PhoA* sequences in particular originated from other eukaryotes than the predominant phytoplankton community members (87-98% "other", **Fig. S9**),

which included several zooplankton species as well as some rhizaria (**Table S8**). Even though *phoA* was much less abundant than phytoplankton AP_{aty} or PDE (other), it was present at similar magnitude as *phoX* and other enzymes. These observations suggest that *phoA* from zooplankton has the potential for influencing bulk APA observations. Moreover, we anticipate that cyanobacteria and heterotrophic bacteria contribute substantially to DOP cycling in the CCE, which should be considered in future work.

Conclusions

Eastern boundary upwelling systems rank among the most productive ocean biomes on earth and provide crucial socioeconomic services for human society, yet is it unclear how their productivity will evolve under future environmental changes (*91*). Recent studies demonstrate that the global primary production of marine phytoplankton is being hampered through multiple nutrient limitation in all surface seawaters of the world's oceans (*92*). Maturing phytoplankton blooms in eastern boundary upwelling regions exhaust dissolved nutrients while advecting offshore. Our study shows that even if P does not limit phytoplankton growth, several taxa experience underlying P stress in these upwelling areas and access the DOP pool to meet P nutritional requirements. In these aged, upwelled waters, Fe-limited diatoms drove observed increases in APA upon N additions through the use of Fe-free atypical AP_{aty} and *phoA*, since excess N exacerbated P demands. In offshore waters bordering the oligotrophic North Pacific subtropical gyre, however, the whole N-limited eukaryotic community contributed to APA, which increased with Fe+N additions through the use of unclassified, possibly Fe-containing PDE (other) by several taxa. Furthermore, diatoms reacted to sole Fe additions by overexpressing the polyphosphate/ATP-dependent NAD kinase *ppnK*. These diverse responses highlight the occupation of different DOP-metabolizing niches by major taxa, as well as the broad functional diversity they apply toward P nutrition. Emerging computational and experimental evidence predicts that the Pacific subtropical gyres are shifting toward P limitation due to climate-change induced ocean stratification (*93*), increasing N fixation (*94*), and anthropogenic N pollution (*34*). Hence, we expect the mechanisms of microbial DOP utilization to become increasingly relevant in sustaining ocean fertility.

Acknowledgements.
The authors thank the captain, crew and science party of the *R/V Sally Ride* and *R/V Roger Revelle* for supporting this work. In particular, we thank Kiefer O. Forsch, Maxwell Fenton, Minerva M. Padilla, Tyler H. Coale and Katherine A. Barbeau who assisted with sample collection. We also thank Michael R. Stukel and Katherine A. Barbeau for their contributions to the overall cruise operations as chief scientists, and Sydney Plummer, Monika Thukral, Stephanie A. Matthews, and Carl H. Lamborg for their assistance with shipboard experiments.

Funding.
This work was supported by the National Science Foundation (NSF) grants, OCE-1026607, OCE-1637632, and OCE-2224726 to the CCE-LTER program, NSF grant OCE-1756884 and Simons Foundation grant 970820 to A.E.A., and NSF grants OCE-1948042, as well as Simons Foundation grant 678537 to J.M.D. Transcriptomics sequencing was supported by the Scripps Institution of Oceanography, Earth Section Small Grant to V.S.

Data availability
Dissolved inorganic nutrients for P2107 are publicly available at the Environmental Data Initiative (EDI) Data Portal (*95*). RNA amplicon sequence data will be made available in as NCBI Sequence Read Archive as BioProject at time of submission. Additional data is available from the authors upon request.

References.

1. C. B. Field, M. J. Behrenfeld, J. T. Randerson, P. Falkowski, Primary Production of the Biosphere: Integrating Terrestrial and Oceanic Components. *Science* **281**, 237-240 (1998). doi: doi:10.1126/science.281.5374.237.
2. S. Duhamel, J. M. Diaz, J. C. Adams, K. Djaoudi, V. Steck, E. M. Waggoner, Phosphorus as an integral component of global marine biogeochemistry. *Nat. Geosci.* **14**, 359-368 (2021). doi: 10.1038/s41561-021-00755-8.
3. S. T. Dyhrman, K. C. Ruttenberg, Presence and regulation of alkaline phosphatase activity in eukaryotic phytoplankton from the coastal ocean: Implications for dissolved organic phosphorus remineralization. *Limnol. Oceanogr.* **51**, 1381-1390 (2006). doi: 10.4319/lo.2006.51.3.1381.
4. H. Luo, H. Zhang, R. A. Long, R. Benner, Depth distributions of alkaline phosphatase and phosphonate utilization genes in the North Pacific Subtropical Gyre. *Aquat. Microb. Ecol.* **62**, 61-69 (2011). doi: 10.3354/ame01458.
5. G. Trommer, A. Leynaert, C. Klein, A. Naegelen, B. Beker, Phytoplankton phosphorus limitation in a North Atlantic coastal ecosystem not predicted by nutrient load. *J. Plankton Res.* **35**, 1207-1219 (2013). doi: 10.1093/plankt/fbt070.
6. P. J. O'Brie, D. Herschlag, Functional Interrelationships in the Alkaline Phosphatase Superfamily: Phosphodiesterase Activity of Escherichia coli Alkaline Phosphatase. *Biochemistry* **40**, 5691-5699 (2001). doi: 10.1021/bi0028892.
7. S. C. Yong, P. Roversi, J. Lillington, F. Rodriguez, M. Krehenbrink, O. B. Zeldin, E. F. Garman, S. M. Lea, B. C. Berks, A complex iron-calcium cofactor catalyzing phosphotransfer chemistry. *Science* **345**, 1170-1173 (2014). doi: 10.1126/science.1254237.
8. F. Rodriguez, J. Lillington, S. Johnson, C. R. Timmel, S. M. Lea, B. C. Berks, Crystal structure of the Bacillus subtilis phosphodiesterase PhoD reveals an iron and calcium-containing active site. *J. Biol. Chem.* **289**, 30889-30899 (2014). doi: 10.1074/jbc.M114.604892.
9. C. L. Wojciechowski, J. P. Cardia, E. R. Kantrowitz, Alkaline phosphatase from the hyperthermophilic bacterium T. maritima requires cobalt for activity. *Protein Sci.* **11**, 903-911 (2002). doi: 10.1110/ps.4260102.
10. C. Mahaffey, S. Reynolds, C. E. Davis, M. C. Lohan, Alkaline phosphatase activity in the subtropical ocean: insights from nutrient, dust and trace metal addition experiments. *Front. Mar. Sci.* **1**, 1-13 (2014). doi: 10.3389/fmars.2014.00073.
11. T. J. Browning, E. P. Achterberg, J. C. Yong, I. Rapp, C. Utermann, A. Engel, C. M. Moore, Iron limitation of microbial phosphorus acquisition in the tropical North Atlantic. *Nat. Commun.* **8**, 1-7 (2017). doi: 10.1038/ncomms15465.
12. S. Duhamel, K. M. Björkman, F. Van Wambeke, T. Moutin, D. M. Karl, Characterization of alkaline phosphatase activity in the North and South Pacific Subtropical Gyres:

Implications for phosphorus cycling. *Limnol. Oceanogr.* **56**, 1244-1254 (2011). doi: 10.4319/lo.2011.56.4.1244.

13. S. Duhamel, S. T. Dyhrman, D. M. Karl, Alkaline phosphatase activity and regulation in the North Pacific Subtropical Gyre. *Limnol. Oceanogr.* **55**, 1414-1425 (2010). doi: 10.4319/lo.2010.55.3.1414.
14. T. D. Jickells, Z. S. An, K. K. Andersen, A. R. Baker, G. Bergametti, N. Brooks, J. J. Cao, P. W. Boyd, R. A. Duce, K. A. Hunter, H. Kawahata, N. Kubilay, J. laRoche, P. S. Liss, N. Mahowald, J. M. Prospero, A. J. Ridgwell, I. Tegen, R. Torres, Global Iron Connections Between Desert Dust, Ocean Biogeochemistry, and Climate. *Science* **308**, 67-71 (2005). doi: doi:10.1126/science.1105959.
15. M. Rouco, K. R. Frischkorn, S. T. Haley, H. Alexander, S. T. Dyhrman, Transcriptional patterns identify resource controls on the diazotroph *Trichodesmium* in the Atlantic and Pacific oceans. *ISME J.* **12**, 1486-1495 (2018). doi: 10.1038/s41396-018-0087-z.
16. C. L. Young, E. D. Ingall, Marine dissolved organic phosphorus composition: insights from samples recovered using combined electrodialysis/reverse osmosis. *Aquat. Geochem.* **16**, 563-574 (2010). doi: 10.1007/s10498-009-9087-y.
17. S. T. Dyhrman, B. D. Jenkins, T. A. Rynearson, M. A. Saito, M. L. Mercier, H. Alexander, L. P. Whitney, A. Drzewianowski, V. V. Bulygin, E. M. Bertrand, Z. Wu, C. Benitez-Nelson, A. Heithoff, The Transcriptome and Proteome of the Diatom *Thalassiosira pseudonana* Reveal a Diverse Phosphorus Stress Response. *PLoS One* **7**, e33768 (2012). doi: 10.1371/journal.pone.0033768.
18. X.-H. Chen, Y.-Y. Li, H. Zhang, J.-L. Liu, Z.-X. Xie, L. Lin, D.-Z. Wang, Quantitative Proteomics Reveals Common and Specific Responses of a Marine Diatom Thalassiosira pseudonana to Different Macronutrient Deficiencies. *Front. Microbiol.* **9**, wrae163 (2018). doi: 10.3389/fmicb.2018.02761.
19. J. M. Diaz, A. Holland, J. G. Sanders, K. Bulski, D. Mollett, C.-W. Chou, D. Phillips, Y. Tang, S. Duhamel, Dissolved Organic Phosphorus Utilization by Phytoplankton Reveals Preferential Degradation of Polyphosphates Over Phosphomonoesters. *Front. Mar. Sci.* **5**, 1-17 (2018). doi: 10.3389/fmars.2018.00380.
20. J. M. Diaz, R. Steffen, J. G. Sanders, Y. Tang, S. Duhamel, Preferential utilization of inorganic polyphosphate over other bioavailable phosphorus sources by the model diatoms *Thalassiosira spp*. *Environ. Microbiol.* **21**, 2415-2425 (2019). doi: 10.1111/1462-2920.14630.
21. E. M. Waggoner, K. Djaoudi, J. M. Diaz, S. Duhamel, Dissolved organic phosphorus bond-class utilization by Synechococcus. *FEMS Microbiol. Ecol.* **100**, fiae099 (2024). doi: 10.1093/femsec/fiae099.
22. L. P. Whitney, M. W. Lomas, Phosphonate utilization by eukaryotic phytoplankton. *Limnol. Oceanogr. Lett.* **4**, 18-24 (2019). doi: 10.1002/lol2.10100.
23. M. Acker, S. L. Hogle, P. M. Berube, T. Hackl, A. Coe, R. Stepanauskas, S. W. Chisholm, D. J. Repeta, Phosphonate production by marine microbes: Exploring new sources and potential function. *Proc. Natl. Acad. Sci.* **119**, e2113386119 (2022). doi: doi:10.1073/pnas.2113386119.
24. P. Martin, S. T. Dyhrman, M. W. Lomas, N. J. Poulton, B. A. S. Van Mooy, Accumulation and enhanced cycling of polyphosphate by Sargasso Sea plankton in response to low phosphorus. *Proc. Natl. Acad. Sci.* **111**, 8089-8094 (2014). doi: 10.1073/pnas.1321719111.

25. B. Temperton, J. A. Gilbert, J. P. Quinn, J. W. McGrath, Novel Analysis of Oceanic Surface Water Metagenomes Suggests Importance of Polyphosphate Metabolism in Oligotrophic Environments. *PLoS One* **6**, e16499 (2011). doi: 10.1371/journal.pone.0016499.
26. J. C. Adams, R. Steffen, C.-W. Chou, S. Duhamel, J. M. Diaz, Dissolved organic phosphorus utilization by the marine bacterium *Ruegeria pomeroyi* DSS-3 reveals chain length-dependent polyphosphate degradation. *Environ. Microbiol.* **24**, 2259-2269 (2022). doi: 10.1111/1462-2920.15877.
27. I. Closset, H. M. McNair, M. A. Brzezinski, J. W. Krause, K. Thamatrakoln, J. L. Jones, Diatom response to alterations in upwelling and nutrient dynamics associated with climate forcing in the California Current System. *Limnol. Oceanogr.* **66**, 1578-1593 (2021). doi: 10.1002/lno.11705.
28. C. Deutsch, H. Frenzel, J. C. McWilliams, L. Renault, F. Kessouri, E. Howard, J.-H. Liang, D. Bianchi, S. Yang, Biogeochemical variability in the California Current System. *Prog. Oceanogr.* **196**, 102565 (2021). doi: 10.1016/j.pocean.2021.102565.
29. S. L. Hogle, C. L. Dupont, B. M. Hopkinson, A. L. King, K. N. Buck, K. L. Roe, R. K. Stuart, A. E. Allen, E. L. Mann, Z. I. Johnson, K. A. Barbeau, Pervasive iron limitation at subsurface chlorophyll maxima of the California Current. *Proc. Natl. Acad. Sci.* **115**, 13300-13305 (2018). doi: 10.1073/pnas.1813192115.
30. D. A. Hutchins, G. R. DiTullio, Y. Zhang, K. W. Bruland, An iron limitation mosaic in the California upwelling regime. *Limnol. Oceanogr.* **43**, 1037-1054 (1998). doi: 10.4319/lo.1998.43.6.1037.
31. California Current Ecosystem - Long Term Ecological Research (CCE-LTER). Accessed Oct 28 2021. doi: http://cce.lternet.edu/data/.
32. R. M. Letelier, K. M. Björkman, M. J. Church, D. S. Hamilton, N. M. Mahowald, R. A. Scanza, N. Schneider, A. E. White, D. M. Karl, Climate-driven oscillation of phosphorus and iron limitation in the North Pacific Subtropical Gyre. *Proc. Natl. Acad. Sci.* **116**, 12720-12728 (2019). doi: 10.1073/pnas.1900789116.
33. R. T. Letscher, J. K. Moore, Preferential remineralization of dissolved organic phosphorus and non-Redfield DOM dynamics in the global ocean: Impacts on marine productivity, nitrogen fixation, and carbon export. *Global Biogeochem. Cycles* **29**, 325-340 (2015). doi: 10.1002/2014GB004904.
34. I.-N. Kim, K. Lee, N. Gruber, D. M. Karl, J. L. Bullister, S. Yang, T.-W. Kim, Increasing anthropogenic nitrogen in the North Pacific Ocean. *Science* **346**, 1102-1106 (2014). doi: 10.1126/science.1258396.
35. M. R. Stukel, M. D. Ohman, C. R. Benitez-Nelson, M. R. Landry, Contributions of mesozooplankton to vertical carbon export in a coastal upwelling system. *Mar. Ecol.: Prog. Ser.* **491**, 47-65 (2013). doi: 10.3354/meps10453.
36. J. D. H. Strickland, T. R. Parsons, *A practical handbook of seawater analysis*. Canadian bulletin of fisheries and aquatic sciences (Fisheries Research Board of Canada, Ottawa, Canada, ed. 2, 1972), vol. 167, pp. 310.
37. R. Schlitzer, Ocean Data View (2025). doi: https://odv.awi.de.
38. CalCOFI Methods Manual. Accessed Mar 06 2025. doi: https://calcofi.org/sampling-info/methods/.
39. A. Rabines, R. H. Lampe, A. E. Allen, Sterivex RNA extraction. Accessed Mar 06 2025 (2020). doi: https://doi.org/10.17504/protocols.io.bd9ti96n.

40. A. M. Bolger, M. Lohse, B. Usadel, Trimmomatic: A flexible trimmer for Illumina Sequence Data. *Bioinformatics* **30**, 2114-2120 (2014). doi: 10.1093/bioinformatics/btu170.
41. P. Ewels, M. Magnusson, S. Lundin, M. Käller, MultiQC: summarize analysis results for multiple tools and samples in a single report. *Bioinformatics* **32**, 3047-3048 (2016). doi: 10.1093/bioinformatics/btw354.
42. E. Bushmanova, D. Antipov, A. Lapidus, A. D. Prjibelski, rnaSPAdes: a de novo transcriptome assembler and its application to RNA-Seq data. *GigaScience* **8**, (2019). doi: 10.1093/gigascience/giz100.
43. D. Li, C.-M. Liu, R. Luo, K. Sadakane, T.-W. Lam, MEGAHIT: an ultra-fast single-node solution for large and complex metagenomics assembly via succinct de Bruijn graph. *Bioinformatics* **31**, 1674-1676 (2015). doi: 10.1093/bioinformatics/btv033.
44. S. Tang, A. Lomsadze, M. Borodovsky, Identification of protein coding regions in RNA transcripts. *Nucleic Acids Res.* **43**, e78 (2015). doi: 10.1093/nar/gkv227.
45. B. Langmead, S. L. Salzberg, Fast gapped-read alignment with Bowtie 2. *Nat. Methods* **9**, 357-359 (2012). doi: 10.1038/nmeth.1923.
46. E. M. Bertrand, J. P. McCrow, A. Moustafa, H. Zheng, J. B. McQuaid, T. O. Delmont, A. F. Post, R. E. Sipler, J. L. Spackeen, K. Xu, D. A. Bronk, D. A. Hutchins, A. E. Allen, Phytoplankton–bacterial interactions mediate micronutrient colimitation at the coastal Antarctic sea ice edge. *Proc. Nat. Acad. Sci. USA* **112**, 9938-9943 (2015). doi: 10.1073/pnas.1501615112.
47. B. Buchfink, C. Xie, D. H. Huson, Fast and sensitive protein alignment using DIAMOND. *Nat. Methods* **12**, 59-60 (2015). doi: 10.1038/nmeth.3176.
48. E. M. Bertrand, J. P. McCrow, A. Moustafa, H. Zheng, J. B. McQuaid, T. O. Delmont, A. F. Post, R. E. Sipler, J. L. Spackeen, K. Xu, D. A. Bronk, D. A. Hutchins, A. E. Allen, Phytoplankton–bacterial interactions mediate micronutrient colimitation at the coastal Antarctic sea ice edge. *Proc. Natl. Acad. Sci. USA* **112**, 9938-9943 (2015). doi: 10.1073/pnas.1501615112.
49. S. Podell, T. Gaasterland, DarkHorse: a method for genome-wide prediction of horizontal gene transfer. *Genome Biology* **8**, R16 (2007). doi: 10.1186/gb-2007-8-2-r16.
50. M. Kanehisa, M. Furumichi, M. Tanabe, Y. Sato, K. Morishima, KEGG: new perspectives on genomes, pathways, diseases and drugs. *Nucleic Acids Res.* **45**, D353-D361 (2017). doi: 10.1093/nar/gkw1092.
51. T. Aramaki, R. Blanc-Mathieu, H. Endo, K. Ohkubo, M. Kanehisa, S. Goto, H. Ogata, KofamKOALA: KEGG Ortholog assignment based on profile HMM and adaptive score threshold. *Bioinformatics* **36**, 2251-2252 (2019). doi: 10.1093/bioinformatics/btz859.
52. M. I. Love, W. Huber, S. Anders, Moderated estimation of fold change and dispersion for RNA-seq data with DESeq2. *Genome Biol.* **15**, 550 (2014). doi: 10.1186/s13059-014-0550-8.
53. A. C. Redfield, in *James Johnstone Memorial Volume*. (University of Liverpool, Liverpool, 1934), pp. 176-192.
54. C. L. Dupont, J. P. McCrow, R. Valas, A. Moustafa, N. Walworth, U. Goodenough, R. Roth, S. L. Hogle, J. Bai, Z. I. Johnson, E. Mann, B. Palenik, K. A. Barbeau, J. Craig Venter, A. E. Allen, Genomes and gene expression across light and productivity gradients in eastern subtropical Pacific microbial communities. *ISME J.* **9**, 1076-1092 (2015). doi: 10.1038/ismej.2014.198.

55. N. G. Walworth, M. A. Saito, M. D. Lee, M. R. McIlvin, D. M. Moran, R. M. Kellogg, F.-X. Fu, D. A. Hutchins, E. A. Webb, Why Environmental Biomarkers Work: Transcriptome–Proteome Correlations and Modeling of Multistressor Experiments in the Marine Bacterium *Trichodesmium*. *J. Proteome Res.* **21**, 77-89 (2022). doi: 10.1021/acs.jproteome.1c00517.
56. N. L. Hockin, T. Mock, F. Mulholland, S. Kopriva, G. Malin, The Response of Diatom Central Carbon Metabolism to Nitrogen Starvation Is Different from That of Green Algae and Higher Plants *Plant Physiol.* **158**, 299-312 (2011). doi: 10.1104/pp.111.184333.
57. S. J. Bender, C. A. Durkin, C. T. Berthiaume, R. L. Morales, E. V. Armbrust, Transcriptional responses of three model diatoms to nitrate limitation of growth. *Front. Mar. Sci.* **1**, (2014). doi: 10.3389/fmars.2014.00003.
58. J. Morrissey, R. Sutak, J. Paz-Yepes, A. Tanaka, A. Moustafa, A. Veluchamy, Y. Thomas, H. Botebol, F.-Y. Bouget, Jeffrey B. McQuaid, L. Tirichine, Andrew E. Allen, E. Lesuisse, C. Bowler, A Novel Protein, Ubiquitous in Marine Phytoplankton, Concentrates Iron at the Cell Surface and Facilitates Uptake. *Curr. Biol.* **25**, 364-371 (2015). doi: 10.1016/j.cub.2014.12.004.
59. J. B. McQuaid, A. B. Kustka, M. Oborník, A. Horák, J. P. McCrow, B. J. Karas, H. Zheng, T. Kindeberg, A. J. Andersson, K. A. Barbeau, A. E. Allen, Carbonate-sensitive phytotransferrin controls high-affinity iron uptake in diatoms. *Nature* **555**, 534-537 (2018). doi: 10.1038/nature25982.
60. J. Behnke, J. LaRoche, Iron uptake proteins in algae and the role of Iron Starvation-Induced Proteins (ISIPs). *Eur. J. Phycol.* **55**, 339-360 (2020). doi: 10.1080/09670262.2020.1744039.
61. J. L. Roche, H. Murray, M. Orellana, J. Newton, Flavodoxin Expression as an Indicator of Iron Limitation in Marine Diatoms. *J. Phycol.* **31**, 520-530 (1995). doi: 10.1111/j.1529-8817.1995.tb02545.x.
62. A. Marchetti, D. M. Schruth, C. A. Durkin, M. S. Parker, R. B. Kodner, C. T. Berthiaume, R. Morales, A. E. Allen, E. V. Armbrust, Comparative metatranscriptomics identifies molecular bases for the physiological responses of phytoplankton to varying iron availability. *Proc. Natl. Acad. Sci.* **109**, E317-E325 (2012). doi: 10.1073/pnas.1118408109.
63. R. M. Kellogg, M. A. Moosburner, N. R. Cohen, N. J. Hawco, M. R. McIlvin, D. M. Moran, G. R. DiTullio, A. V. Subhas, A. E. Allen, M. A. Saito, Adaptive responses of marine diatoms to zinc scarcity and ecological implications. *Nat. Commun.* **13**, 1995 (2022). doi: 10.1038/s41467-022-29603-y.
64. R. M. Kell, A. V. Subhas, N. L. Schanke, L. E. Lees, R. J. Chmiel, D. Rao, M. M. Brisbin, D. M. Moran, M. R. McIlvin, F. Bolinesi, O. Mangoni, R. Casotti, C. Balestra, T. J. Horner, R. B. Dunbar, A. E. Allen, G. R. DiTullio, M. A. Saito, Zinc stimulation of phytoplankton in a low carbon dioxide, coastal Antarctic environment. *bioRxiv*, 2023.2011.2005.565706 (2024). doi: 10.1101/2023.11.05.565706.
65. M. A. Saito, M. R. McIlvin, D. M. Moran, T. J. Goepfert, G. R. DiTullio, A. F. Post, C. H. Lamborg, Multiple nutrient stresses at intersecting Pacific Ocean biomes detected by protein biomarkers. *Science* **345**, 1173-1177 (2014). doi: 10.1126/science.1256450.
66. H. Matsui, H. Harada, K. Maeda, T. Sugiyama, Y. Fukuchi, N. Kimura, H. Nawaly, Y. Tsuji, Y. Matsuda, Coordinated phosphate uptake by extracellular alkaline phosphatase and solute carrier transporters in marine diatoms. *New Phytologist* **241**, 1210-1221 (2024). doi: 10.1111/nph.19410.

67. L. L. Wurch, E. M. Bertrand, M. A. Saito, B. A. S. Van Mooy, S. T. Dyhrman, Proteome Changes Driven by Phosphorus Deficiency and Recovery in the Brown Tide-Forming Alga *Aureococcus anophagefferens*. *PLoS One* **6**, e28949 (2011). doi: 10.1371/journal.pone.0028949.
68. N. R. Cohen, H. Alexander, A. I. Krinos, S. K. Hu, R. H. Lampe, Marine Microeukaryote Metatranscriptomics: Sample Processing and Bioinformatic Workflow Recommendations for Ecological Applications. *Front. Mar. Sci.* **9**, (2022). doi: 10.3389/fmars.2022.867007.
69. X. Lin, L. Wang, X. Shi, S. Lin, Rapidly diverging evolution of an atypical alkaline phosphatase (PhoAaty) in marine phytoplankton: insights from dinoflagellate alkaline phosphatases. *Front. Microbiol.* **6**, (2015). doi: 10.3389/fmicb.2015.00868.
70. T. Li, C. Guo, Y. Zhang, C. Wang, X. Lin, S. Lin, Identification and Expression Analysis of an Atypical Alkaline Phosphatase in *Emiliania huxleyi*. *Front. Microbiol.* **9**, (2018). doi: 10.3389/fmicb.2018.02156.
71. A. Torcello-Requena, A. R. J. Murphy, I. D. E. A. Lidbury, F. D. Pitt, R. Stark, A. D. Millard, R. J. Puxty, Y. Chen, D. J. Scanlan, A distinct, high-affinity, alkaline phosphatase facilitates occupation of P-depleted environments by marine picocyanobacteria. *Proc. Natl. Acad. Sci.* **121**, e2312892121 (2024). doi: doi:10.1073/pnas.2312892121.
72. M. Sato, R. Sakuraba, F. Hashihama, Phosphate monoesterase and diesterase activities in the North and South Pacific Ocean. *Biogeosciences* **10**, 7677-7688 (2013). doi: 10.5194/bg-10-7677-2013.
73. M. Sebastián, J. Arístegui, M. F. Montero, J. Escanez, F. Xavier Niell, Alkaline phosphatase activity and its relationship to inorganic phosphorus in the transition zone of the North-western African upwelling system. *Prog. Oceanogr.* **62**, 131-150 (2004). doi: 10.1016/j.pocean.2004.07.007.
74. C. E. Davis, C. Mahaffey, Elevated alkaline phosphatase activity in a phosphate-replete environment: Influence of sinking particles. *Limnol. Oceanogr.* **62**, 2389-2403 (2017). doi: 10.1002/lno.10572.
75. I. D. E. A. Lidbury, D. J. Scanlan, A. R. J. Murphy, J. A. Christie-Oleza, M. M. Aguilo-Ferretjans, A. Hitchcock, T. J. Daniell, A widely distributed phosphate-insensitive phosphatase presents a route for rapid organophosphorus remineralization in the biosphere. *Proc. Natl. Acad. Sci.* **119**, e2118122119 (2022). doi: 10.1073/pnas.2118122119.
76. B. Thomson, J. Wenley, K. Currie, C. Hepburn, G. J. Herndl, F. Baltar, Resolving the paradox: Continuous cell-free alkaline phosphatase activity despite high phosphate concentrations. *Mar. Chem.* **214**, 103671 (2019). doi: 10.1016/j.marchem.2019.103671.
77. J. W. Ammerman, F. Azam, Bacterial 5'-nucleotidase activity in estuarine and coastal marine waters: Characterization of enzyme activity. *Limnol. Oceanogr.* **36**, 1427-1436 (1991). doi: 10.4319/lo.1991.36.7.1427.
78. E. Cerdan-Garcia, A. Baylay, D. Polyviou, E. M. S. Woodward, L. Wrightson, C. Mahaffey, M. C. Lohan, C. M. Moore, T. S. Bibby, J. C. Robidart, Transcriptional responses of Trichodesmium to natural inverse gradients of Fe and P availability. *ISME J.* **16**, 1055-1064 (2021). doi: 10.1038/s41396-021-01151-1.
79. M. Suzumura, F. Hashihama, N. Yamada, S. Kinouchi, Dissolved Phosphorus Pools and Alkaline Phosphatase Activity in the Euphotic Zone of the Western North Pacific Ocean. *Front. Microbiol.* **3**, (2012). doi: 10.3389/fmicb.2012.00099.
80. K. O. Forsch, K. C. Fulton, M. M. Weiss, J. W. Krause, M. R. Stukel, K. A. Barbeau, Iron limitation and biogeochemical effects in southern California current coastal upwelling

filaments. *J. Geophys. Res.: Oceans* **128**, e2023JC019961 (2023). doi: 10.1029/2023JC019961.

81. S. Y. McLoughlin, C. Jackson, J.-W. Liu, D. L. Ollis, Growth of *Escherichia coli* Coexpressing Phosphotriesterase and Glycerophosphodiester Phosphodiesterase, Using Paraoxon as the Sole Phosphorus Source. *Appl. Environ. Microbiol.* **70**, 404-412 (2004). doi: 10.1128/AEM.70.1.404-412.2004.
82. C. L. Myers, R. G. Ireland, T. A. Garrett, E. D. Brown, Characterization of Wall Teichoic Acid Degradation by the Bacteriophage ϕ29 Appendage Protein GP12 Using Synthetic Substrate Analogs. *J. Biol. Chem.* **290**, 19133-19145 (2015). doi: 10.1074/jbc.M115.662866.
83. N. Matange, M. Podobnik, Sandhya S. Visweswariah, Metallophosphoesterases: structural fidelity with functional promiscuity. *Biochem. J.* **467**, 201-216 (2015). doi: 10.1042/bj20150028.
84. A. C. Darby, A. C. Gill, S. D. Armstrong, C. S. Hartley, D. Xia, J. M. Wastling, B. L. Makepeace, Integrated transcriptomic and proteomic analysis of the global response of Wolbachia to doxycycline-induced stress. *ISME J.* **8**, 925-937 (2013). doi: 10.1038/ismej.2013.192.
85. D. J. Jamieson, Oxidative stress responses of the yeast Saccharomyces cerevisiae. *Yeast* **14**, 1511-1527 (1998). doi: 10.1002/(SICI)1097-0061(199812)14:16<1511::AID-YEA356>3.0.CO;2-S.
86. Y. Xu, S. K. K. Leung, T. M. W. Li, C. C. M. Yung, Hidden genomic diversity drives niche partitioning in a cosmopolitan eukaryotic picophytoplankton. *ISME J.* **18**, (2024). doi: 10.1093/ismejo/wrae163.
87. N. Guérin, M. Ciccarella, E. Flamant, P. Frémont, S. Mangenot, B. Istace, B. Noel, C. Belser, L. Bertrand, K. Labadie, C. Cruaud, S. Romac, C. Bachy, M. Gachenot, E. Pelletier, A. Alberti, O. Jaillon, P. Wincker, J.-M. Aury, Q. Carradec, Genomic adaptation of the picoeukaryote Pelagomonas calceolata to iron-poor oceans revealed by a chromosome-scale genome sequence. *Commun. Biol.* **5**, 983 (2022). doi: 10.1038/s42003-022-03939-z.
88. O. A. Sosa, D. J. Repeta, E. F. DeLong, M. D. Ashkezari, D. M. Karl, Phosphate-limited ocean regions select for bacterial populations enriched in the carbon–phosphorus lyase pathway for phosphonate degradation. *Environ. Microbiol.* **21**, 2402-2414 (2019). doi: 10.1111/1462-2920.14628.
89. B. N. Granzow, O. A. Sosa, M. Gonnelli, C. Santinelli, D. M. Karl, D. J. Repeta, A sensitive fluorescent assay for measuring carbon-phosphorus lyase activity in aquatic systems. *Limnol. Oceanogr.: Methods* **19**, 235-244 (2021). doi: 10.1002/lom3.10418.
90. C. Davis, M. C. Lohan, R. Tuerena, E. Cerdan-Garcia, E. M. S. Woodward, A. Tagliabue, C. Mahaffey, Diurnal variability in alkaline phosphatase activity and the potential role of zooplankton. *Limnology and Oceanography Letters* **4**, 71-78 (2019). doi: 10.1002/lol2.10104.
91. S. J. Bograd, M. G. Jacox, E. L. Hazen, E. Lovecchio, I. Montes, M. Pozo Buil, L. J. Shannon, W. J. Sydeman, R. R. Rykaczewski, Climate Change Impacts on Eastern Boundary Upwelling Systems. *Annu. Rev. Mar. Sci.* **15**, 303-328 (2023). doi: 10.1146/annurev-marine-032122-021945.
92. T. J. Browning, C. M. Moore, Global analysis of ocean phytoplankton nutrient limitation reveals high prevalence of co-limitation. *Nat. Commun.* **14**, 5014 (2023). doi: 10.1038/s41467-023-40774-0.

93. S. Gerace, J. Yu, J. K. Moore, A. C. Martiny, Observed declines in upper ocean phosphate-to-nitrate availability. *Proc. Natl. Acad. Sci. U.S.A.* **122**, e2411835122 (2025). doi: 10.1073/pnas.2411835122.
94. D. Karl, R. Letelier, L. Tupas, J. Dore, J. Christian, D. Hebel, The role of nitrogen fixation in biogeochemical cycling in the subtropical North Pacific Ocean. *Nature* **388**, 533-538 (1997). doi: 10.1038/41474.
95. C. C. E. LTER, R. Goericke, Dissolved inorganic nutrients from CCE LTER process cruises, including 5 macro nutrients from water column bottle sample, 2006 - 2019 (ongoing). *Environmental Data Initiative* **ver 7**, (2022). doi: 10.6073/pasta/0e9975846c4bacf6deae5a3f53c6f9e1.

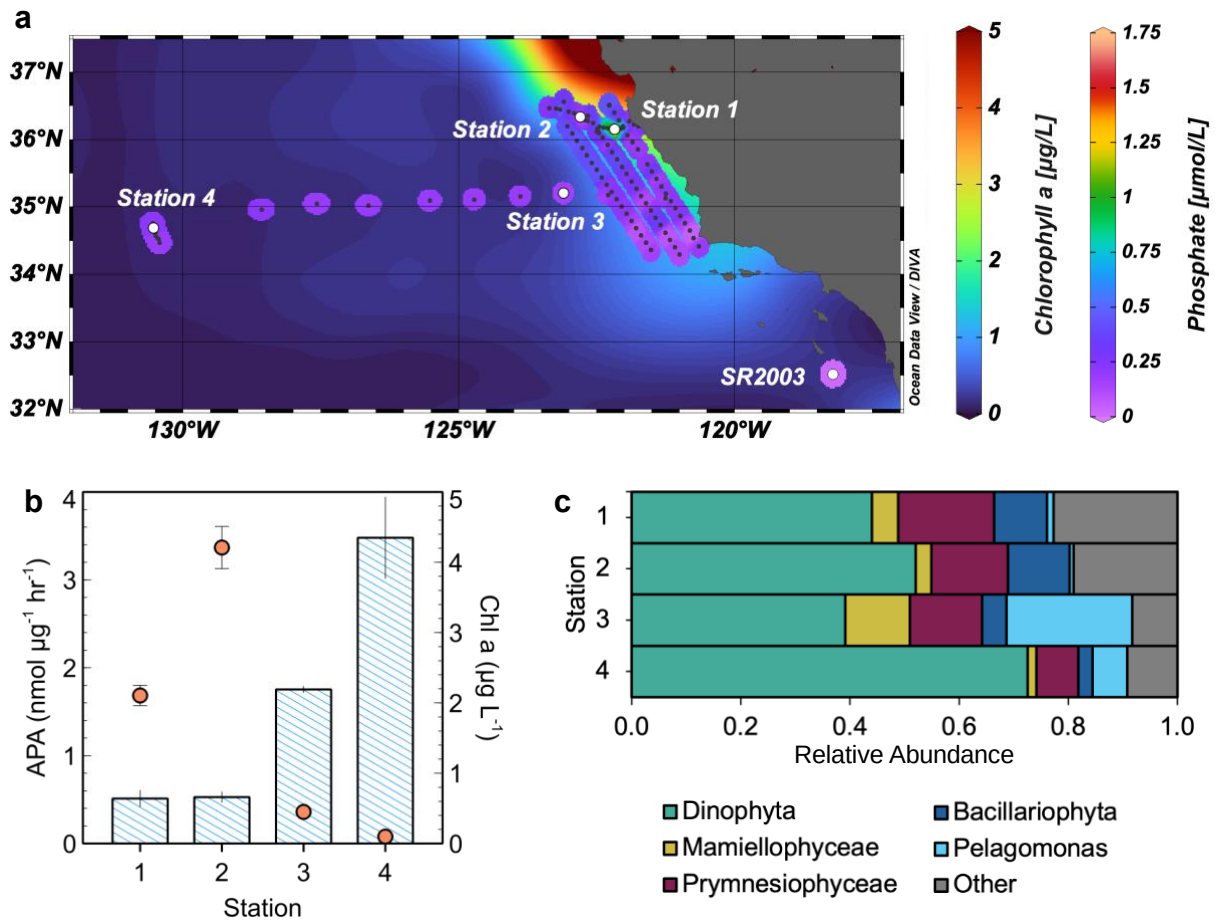

Figure 1. Cruise track, ambient biogeochemical parameters, and eukaryotic community composition in the California Current Ecosystem. a) Surface inorganic phosphate (Pi or PO_4^{3-}; gridded projection) concentrations during the survey transect (black dots) and at stations 1-4 (white circles) on the backdrop of satellite-derived surface chlorophyll a (Chl *a*; contoured background). **b)** *In situ* alkaline phosphatase activity (APA; blue bars) and chlorophyll *a* (Chl *a*; orange circles) at stations 1 (15 m), 2 (20 m), 3 (40 m), and 4 (140 m). Error bars represent one standard error of the mean, $n = 3$. **c)** Average relative abundances of major photosynthetic eukaryotic groups at ambient conditions inferred from poly(A)-selected mRNA (metatranscriptome). The average abundances were derived from the relative abundances of eukaryotic-assigned transcripts per million normalized reads (TPM).

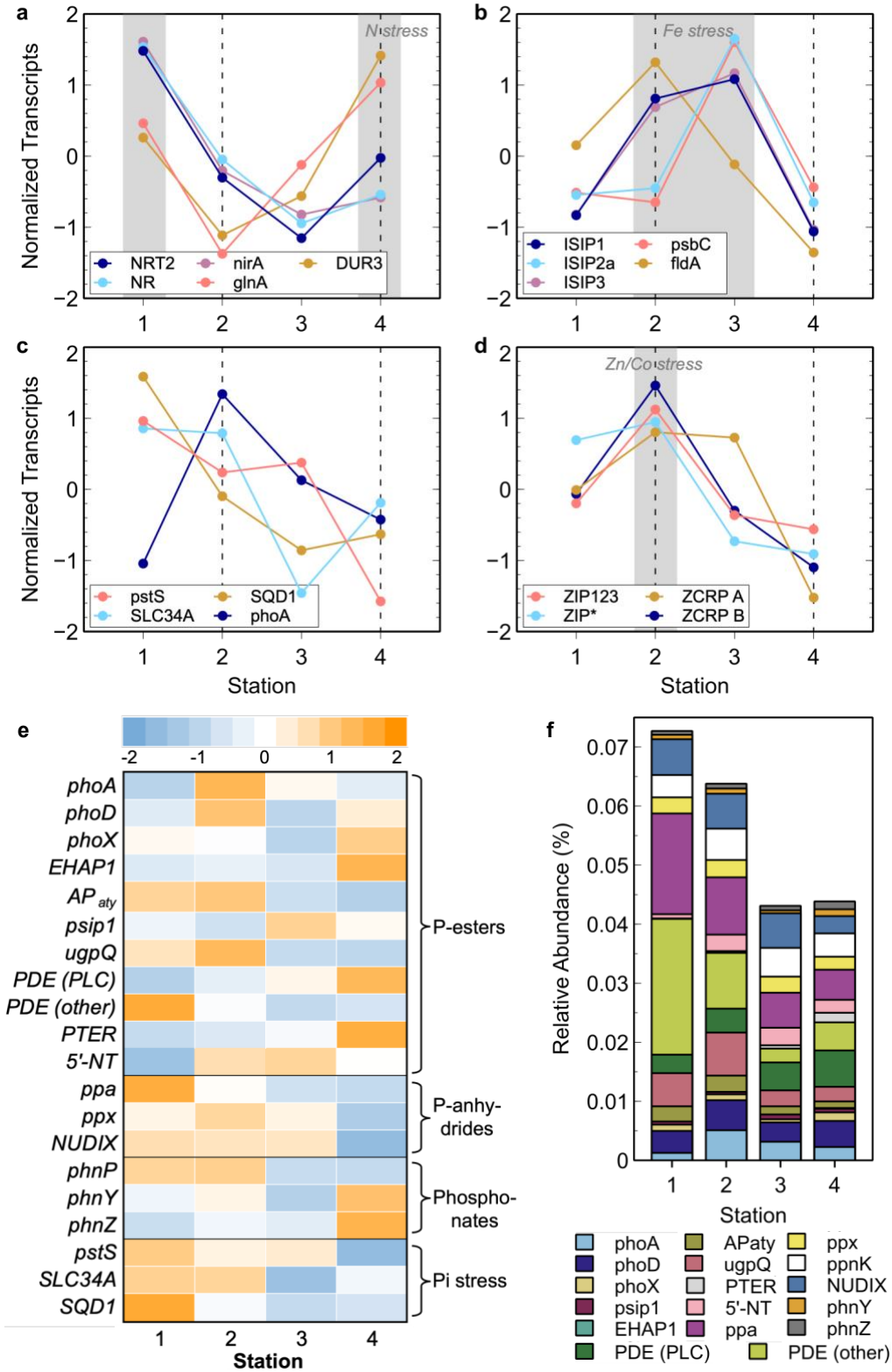

Figure 2. *In situ* transcriptomic signatures of phytoplankton community nutrient stress at stations 1-4. Established stress biomarkers for nitrogen (N; **a**), iron (Fe; **b**), phosphorus (P; **c**) and zinc/cobalt (Zn/Co; **d**) as z-score normalized relative abundances (%) of transcripts per million. Dotted lines indicate stations selected for bioassays; shaded areas denote inferred nutrient stress.

(**e**) Heatmap depicts z-score normalized percentages of transcripts involved in P metabolism. (**f**) Relative abundances of DOP hydrolase transcripts. NRT2, nitrate/nitrite transporter; NR, NAD(P)H-nitrate reductase; *nirA*, ferredoxin-nitrite reductase; *glnA*, glutamine synthetase; DUR3, urea-proton symporter; ISIP1-3, iron stress responsive proteins 1-3; *psbC*, photosystem II CP43 chlorophyll apoprotein; *fldA*, flavodoxin A; *pstS*, high-affinity phosphate transport system substrate-binding protein; SLC34A, sodium-dependent phosphate cotransporter; SQD1, UDP-sulfoquinovose synthase; *phoA*, alkaline phosphatase PhoA; ZIP123 and ZIP8, solute carrier family 39 (zinc transporter); ZCRP A/B, zinc/cobalt responsive proteins A/B; *phoD*, alkaline phosphatase PhoD; *phoX*, alkaline phosphatase PhoX; EHAP1, *Emiliania huxleyi* AP1; AP_{aty}, atypical alkaline phosphatase; *psip1*, alkaline phosphatase Psip1; *ugpQ*, glycerophosphoryl diester phosphodiesterase; PDE (PLC), PLC-like phosphodiesterase; PDE (other), unclassified phosphodiesterase; PTER, phosphotriesterases; 5NT, 5'-nucleotidases; *ppa*, inorganic pyrophosphatase; *ppx*, exopolyphosphatase; *nudH*, (di)nucleoside polyphosphate hydrolase; NUDIX, 8-oxo-dGTP diphosphatase; *phnP*, phosphonate regulator; *phnY*, 2-aminoethylphosphonate dioxygenase; *phnZ*, 2-amino-1-hydroxyethylphosphonate dioxygenase.

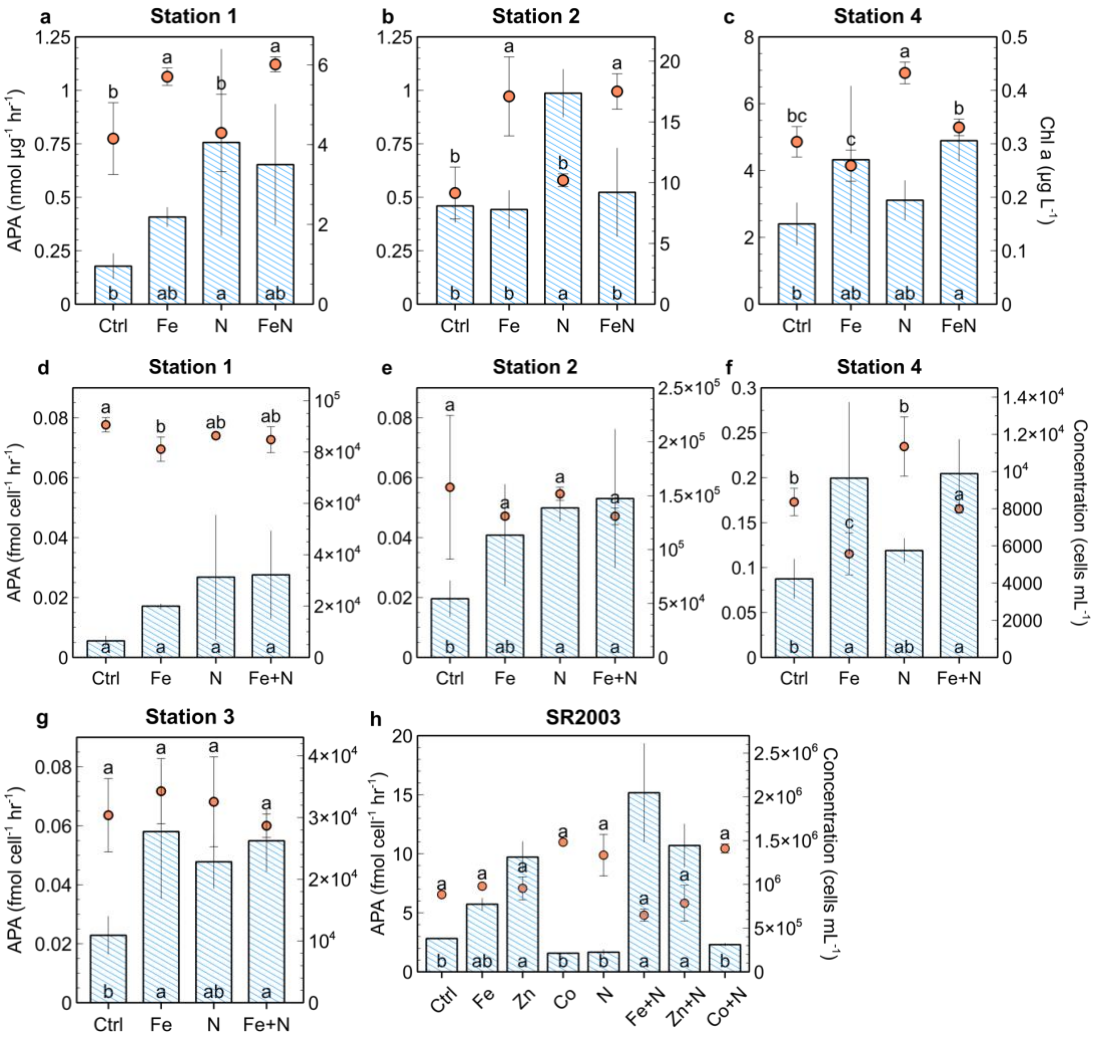

Figure 3. Microbial growth and alkaline phosphatase activity (APA) at experiment locations in the CCE. Microbial biomass (orange circles) and normalized APA (blue bars) using chlorophyll (Chl *a*; **a-c**), phytoplankton counts (cells mL^{-1}; **d-g**), or total microorganism counts (cells mL^{-1}; **h**) at stations 1-4 and SR2003. Treatments lacking a shared letter are significantly different (paired t-test, $p < 0.05$). Error bars represent one standard error of the mean, n = 3 (**a-g**), 2 (**h**).

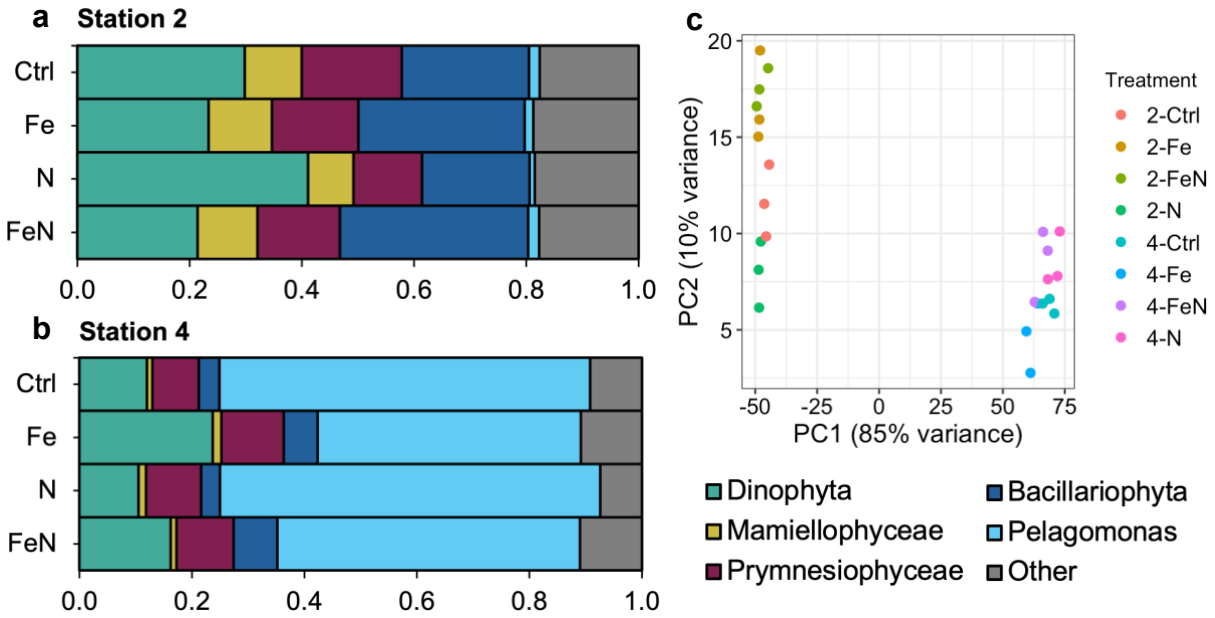

Figure 4. Microbial community responses to metal additions during incubation experiments in the CCE. a) Average relative abundances of major photosynthetic eukaryotic groups bottle incubations at stations 2 and 4 inferred from poly(A)-selected mRNA (metatranscriptome). The average abundances were derived from the relative abundances of eukaryotic-assigned transcripts per million normalized reads (TPM). **b)** Principal Component Analysis (PCA) plots for eukaryotic mRNA within incubation experiments. Stations and treatments are denoted by color as described in the legend.

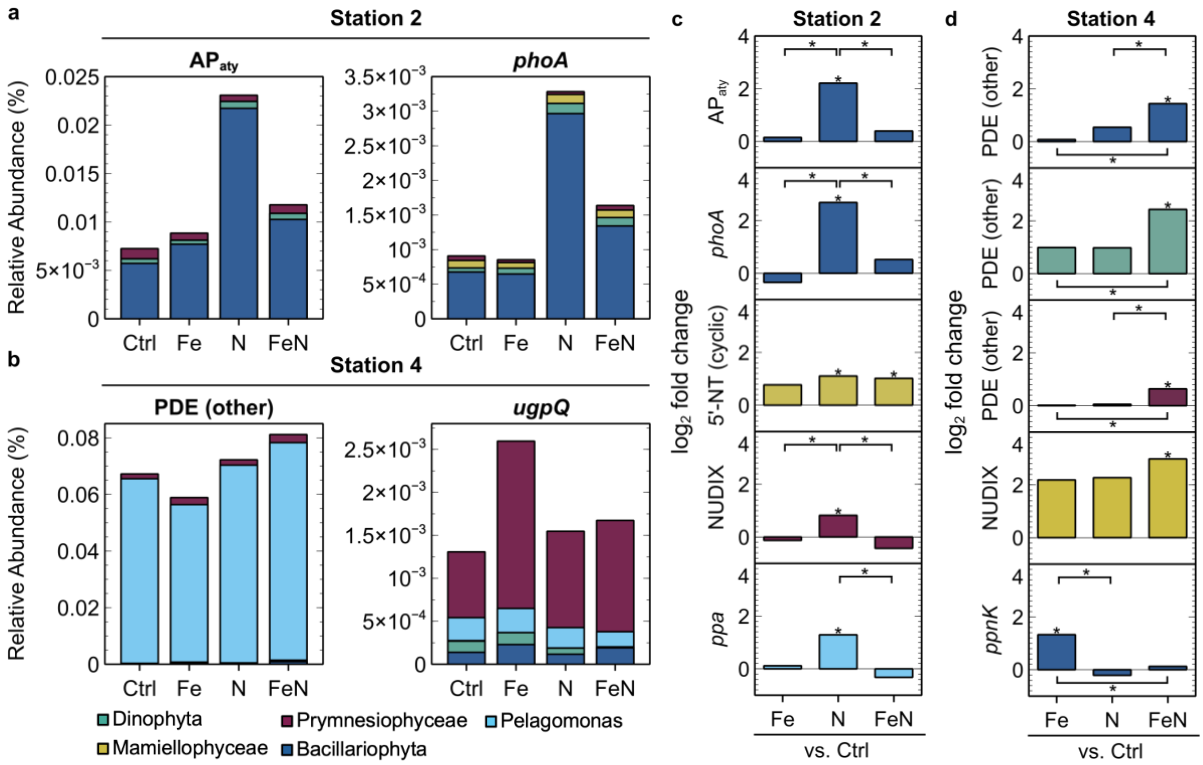

Figure 5. Taxon-specific transcript abundance and differential expression of phosphatases within incubation experiments. Relative abundance (%) of transcripts per million (**a, b**) and differentially expressed transcripts as log2-fold change proportion of expression (**c, d**) for major phytoplankton groups present. Fold-changes denoted with * were deemed statistically significant with an adjusted p-value < 0.05 (DESeq2 Wald test, Benjamini & Hochberg). Gene abbreviations are listed in **Fig. 3**.